https://doi.org/10.5194/acp-2022-213
Preprint. Discussion started: 4 April 2022

Atmospheric Chemistry and Physics Discussions

Radical chemistry at a UK coastal receptor site – Part 2: experimental radical budgets and ozone production

Robert Woodward-Massey[1], Roberto Sommariva[2,4], Lisa K. Whalley[1,3], Danny R. Cryer[1], Trevor Ingham[1], William J. Bloss[4], Stephen M. Ball[2], James D. Lee[5,6], Chris P. Reed[5,a], Leigh R. Crilley[4,b], Louisa J. Kramer[4,c], Brian J. Bandy[7], Grant L. Forster[8], Claire E. Reeves[7], Paul S. Monks[2], and Dwayne E. Heard[1]

[1]School of Chemistry, University of Leeds, Leeds, LS2 9JT, UK
[2]School of Chemistry, University of Leicester, University Road, Leicester, LE1 7RH, UK
[3]National Centre for Atmospheric Science, University of Leeds, Leeds, LS2 9JT, UK
[4]School of Geography, Earth and Environmental Sciences, University of Birmingham, Birmingham, B15 2TT, UK
[5]Wolfson Atmospheric Chemistry Laboratories, Department of Chemistry, University of York, York, YO10 5DD, UK
[6]National Centre for Atmospheric Science, University of York, York, YO10 5DD, UK
[7]Centre for Ocean and Atmospheric Sciences, School of Environmental Sciences, University of East Anglia, Norwich, UK
[8]National Centre for Atmospheric Science, University of East Anglia, Norwich, NR4 7TJ, UK
[a]now at: Faculty for Airborne Atmospheric Measurements, Cranfield University, Cranfield, MK43 0AL, UK
[b]now at: Department of Chemistry, York University, Toronto, M3J 1P3, Canada
[c]now at: Ricardo Energy & Environment, Harwell, Oxfordshire, OX11 0QR, UK

Correspondence to: Lisa K. Whalley (l.k.whalley@leeds.ac.uk) and Dwayne E. Heard (d.e.heard@leeds.ac.uk)

Abstract. In our companion paper (Woodward-Massey et al., 2022), we presented measurements of radical species and OH reactivity (k'_{OH}) made in summer 2015 during the ICOZA (Integrated Chemistry of OZone in the Atmosphere) field campaign at the Weybourne Atmospheric Observatory, a site on the east coast of the UK. In the present work, we used the simultaneous measurement of OH, HO_2, total RO_2, and k'_{OH} to derive experimental (i.e., observationally determined) budgets for all radical species as well as total RO_x (= OH + HO_2 + RO_2). Data were separated according to wind direction: prevailing SW winds (with influence from London and other major conurbations), and all other winds (NW–SE; predominantly marine in origin). In NW–SE air, the RO_x budget could be closed during the daytime within experimental uncertainty but OH destruction exceeded OH production, and HO_2 production greatly exceeded HO_2 destruction while the opposite was true for RO_2. In SW air, the RO_x budget analysis indicated missing daytime RO_x sources but the OH budget was balanced, and the same imbalances were found with the HO_2 and RO_2 budgets as in NW–SE air. For HO_2 and RO_2, the budget imbalances were most severe at high NO mixing ratios.

We explored several mechanistic modifications to the experimental budgets to try to reconcile the HO_2 and RO_2 budget imbalances: (1) the addition of generic radical recycling processes, (2) reduction of the rate of $RO_2 \rightarrow HO_2$ conversion, (3) inclusion of heterogeneous HO_2 uptake, and (4) addition of chlorine chemistry. The best agreement between HO_2 and RO_2 production and destruction rates was found for option (2), in which we reduced the RO_2 + NO rate constant by a factor of 5.

https://doi.org/10.5194/acp-2022-213
Preprint. Discussion started: 4 April 2022

Atmospheric Chemistry and Physics Discussions

The rate of *in situ* ozone production ($P(O_x)$) was calculated from observations of RO_x, NO, and NO_2 and compared to that calculated from MCM-modelled radical concentrations. The MCM-calculated $P(O_x)$ significantly underpredicted the measurement-calculated $P(O_x)$ in the morning, and the degree of underprediction was found to scale with NO.

1 Introduction

The oxidation of volatile organic compounds in the troposphere is controlled by reaction cycles involving the hydroxyl radical (OH), hydroperoxyl radical (HO_2), and organic peroxy radicals (RO_2), collectively known as RO_x. As a consequence of their high reactivities, RO_x species have short chemical lifetimes, less than a second for OH and on the order of a minute for HO_2 and RO_2, and are thus expected to be in photostationary steady-state, where their rates of production are equal to their rates of destruction (i.e., there is budget balance). Historically, measured ambient RO_x concentrations have been compared to simulated concentrations obtained using chemical box models (Stone et al., 2012), which force budget balance. However, recently Tan et al. (2019) showed that, provided RO_x observations are available along with simultaneous supporting measurements (trace gas mixing ratios, photolysis rates, etc.), experimental budgets can be derived for all measured radical species, previously done for OH only. Budget imbalances can be identified with such an approach, and would indicate problems with experimental input data, such as radical concentrations and rate constants, and/or an incorrect chemical mechanism.

In most cases of field campaigns in which radical chemistry was a key focus and measurement-model comparisons were performed, only OH and HO_2 radicals were measured (Stone et al., 2012; Griffith et al., 2013; Hens et al., 2014; Brune et al., 2016; Feiner et al., 2016; Griffith et al., 2016; Mallik et al., 2018). In many campaigns, OH reactivity (k'_{OH}, the inverse of the OH chemical lifetime) observations were also available, which were used to calculate the total OH loss rate and thus allowed for the experimental OH budget to be assessed (e.g., Whalley et al. (2011); Feiner et al. (2016)). However, such studies may also have been impacted by interferences in both OH (Mao et al., 2012; Novelli et al., 2014; Woodward-Massey et al., 2020) and HO_2 (Fuchs et al., 2011; Whalley et al., 2013) detection. More recently, field campaigns have been conducted in which OH, HO_2, RO_2 (facilitated by the advent of the RO_xLIF technique (Fuchs et al., 2008)), and k'_{OH} measurements were all available (Tan et al., 2017; Tan et al., 2018; Whalley et al., 2018; Tan et al., 2019; Slater et al., 2020; Whalley et al., 2020). Tan et al. (2019) showed that such a complete measurement suite allows for the experimental budgets for all radical species to be assessed, and derived budget equations for the sum of RO_x as well as each individual RO_x species.

In our companion paper (Woodward-Massey et al., 2022), we reported OH, HO_2, RO_2, and k'_{OH} observations made during the ICOZA (Integrated Chemistry of OZone in the Atmosphere) field campaign, and compared these to simulations using an MCMv3.3.1 box model. We found significant discrepancies between measured and modelled radical concentrations, particularly under high NO conditions. In the present work, we apply the experimental budget approach of Tan et al. (2019) to the radical measurements. Interference-free measurements of OH were used (Woodward-Massey et al., 2020), and interferences in HO_2 detection were minimised. We show that large imbalances exist between experimental radical production

https://doi.org/10.5194/acp-2022-213
Preprint. Discussion started: 4 April 2022


Atmospheric Chemistry and Physics Discussions

and destruction rates, and suggest explanations for such differences. In addition, we use the measured radical data to calculate *in situ* ozone production rates, and compare these to those calculated from modelled radical concentrations.

2 Methodology

The ICOZA field campaign, described in more detail in our companion paper (Woodward-Massey et al., 2022), took place at the Weybourne Atmospheric Observatory (WAO), located on the North Norfolk Coast, UK (52°57'02" N, 1°07'19"E), approximately 180 km NE of London. A variety of instrumentation was involved in the measurement of trace gases, aerosols, and photolysis frequencies (see Table 1 in (Woodward-Massey et al., 2022)). OH radicals were measured using the fluorescence assay by gas expansion (FAGE) technique (Hard et al., 1984), where for approximately half of the campaign the instrument was equipped with an inlet pre-injector (IPI) for the measurement of OH interferences (Woodward-Massey et al., 2020). HO_2 and RO_2 radicals were measured after chemical conversion to OH using the RO_xLIF method (Fuchs et al., 2008; Fuchs et al., 2011; Whalley et al., 2013). OH reactivity (k'_{OH}) was measured using the laser flash photolysis pump and probe technique (Jeanneret et al., 2001; Sadanaga et al., 2004), where details may be found in (Stone et al., 2016). Trace gas measurements included CO, NO, NO_2, O_3, SO_2, HONO, HCHO, $ClNO_2$, VOCs, and oxygenated VOCs (OVOCs). Aerosol number concentrations and surface areas were measured using an aerodynamic particle sizer (APS). Photolysis rates (J) were measured using a 2π spectral radiometer with $J(O^1D)$ also measured using a 2π filter radiometer (Bohn et al., 2008; Bohn et al., 2016). The chemical and meteorological conditions encountered during ICOZA are summarised in our companion paper (Woodward-Massey et al., 2022). As described in our companion paper, we have split all data according to wind direction: SW winds (180°–270°), and all other winds (NW–SE, <165° and >285°). All data were averaged to 15 minutes prior to performing the analyses featured in this work.

2.1 Radical budget equations

OH, HO_2, RO_2, and k'_{OH} were all measured simultaneously along with relevant supporting measurements (e.g., O_3, NO, HONO, photolysis frequencies, etc.). It is therefore possible to carry out experimental budget analyses for OH, HO_2, and RO_2 as well as their sum, RO_x. This approach was first described by Tan et al. (2019) for measurements made in the Pearl River Delta, China, although many previous studies have investigated the experimental budget of OH only (e.g., Whalley et al. (2011)). Given the short lifetimes of OH, HO_2, and RO_2 radicals (on the order of seconds to minutes), we can assume that their concentrations are in steady-state and hence expect their production and destruction rates to be equal at a location such as the WAO where incoming air is homogeneous. In this section, we describe the reactions involved in RO_x initiation and termination as well as those that interconvert different RO_x species (i.e., propagation). We then show how such reactions can be used to derive budget equations (i.e., production and destruction rates) for all radical species. All reaction rate constants and branching ratios were taken from the Master Chemical Mechanism, MCMv3.3.1 (http://mcm.leeds.ac.uk/MCM/; (Jenkin et al., 2003; Jenkin et al., 2015)).

https://doi.org/10.5194/acp-2022-213
Preprint. Discussion started: 4 April 2022

Atmospheric Chemistry and Physics Discussions

2.1.1 Total $RO_x = OH + HO_2 + RO_2$

RO_x production is driven by the photolysis of O_3, HONO, and OVOCs as well as alkene ozonolysis reactions:

$$O_3 + h\nu\ (\lambda < 340\ \text{nm}) \rightarrow O(^1D) + O_2 \quad \text{(R1a)}$$

$$O(^1D) + H_2O \rightarrow OH + OH \quad \text{(R1b)}$$

$$O(^1D) + M \rightarrow O(^3P) + M \quad \text{(R1c)}$$

$$HONO + h\nu\ (\lambda < 400\ \text{nm}) \rightarrow OH + NO \quad \text{(R2)}$$

$$OVOCs + h\nu \rightarrow HO_2, RO_2 + \text{products} \quad \text{(R3)}$$

$$\text{Alkenes} + O_3 \rightarrow OH, HO_2, RO_2 + \text{products} \quad \text{(R4)}$$

Other photolabile radical reservoir species, such as H_2O_2, ROOH, HNO_3, and $RONO_2$ were not measured during ICOZA and therefore were not considered in RO_x production. The total RO_x production rate may therefore be approximated using:

$$P_{ROx} = 2J(O^1D)[O_3]\,f + J(HONO)[HONO] + \Sigma^i(J(OVOC_i)[OVOC_i](Y^{HO2}{}_{OVOCi} + Y^{RO2}{}_{OVOCi})) + \Sigma^j(k^j{}_4[O_3][ALK_j](Y^{OH}{}_{ALKj} + Y^{HO2}{}_{ALKj} + Y^{RO2}{}_{ALKj})), \quad \text{(E1)}$$

where f is the fraction of $O(^1D)$ atoms that react with H_2O to form OH, $Y^{HO2}{}_{OVOCi}$ and $Y^{RO2}{}_{OVOCi}$ are the HO_2 and RO_2 radical yields from the photolysis of OVOC i, respectively, and $Y^{OH}{}_{ALKj}$, $Y^{HO2}{}_{ALKj}$, and $Y^{RO2}{}_{ALKj}$ are the radical yields from the ozonolysis of alkene (ALK) j. Of the OVOCs measured during ICOZA, those included in equation (E1) were formaldehyde (that photolyses to form HO_2), acetaldehyde (HO_2 and RO_2), and acetone (RO_2). All measured alkenes were included in equation (E1).

RO_x termination is controlled by radical loss to NO_x and the self- and cross-reactions of peroxy radicals:

$$OH + NO \rightarrow HONO \quad \text{(R5)}$$

$$OH + NO_2 \rightarrow HNO_3 \quad \text{(R6)}$$

$$RO_2 + NO \rightarrow RONO_2 \quad \text{(R7)}$$

$$HO_2 + HO_2 \rightarrow H_2O_2 + O_2 \quad \text{(R8a)}$$

$$HO_2 + HO_2 + H_2O \rightarrow H_2O_2 + H_2O + O_2 \quad \text{(R8b)}$$

$$RO_2 + RO_2 \rightarrow \text{products} \quad \text{(R9)}$$

$$RO_2 + HO_2 \rightarrow ROOH + O_2 \quad \text{(R10)}$$

The total RO_x destruction rate is thus given by:

https://doi.org/10.5194/acp-2022-213
Preprint. Discussion started: 4 April 2022


Atmospheric Chemistry and Physics Discussions

$$D_{ROx} = (k_5[NO] + k_6[NO_2])[OH] + k_7[NO][RO_2] + 2(k_8[HO_2]^2 + k_9[RO_2]^2 + k_{10}[RO_2][HO_2]) \quad \text{(E2)}$$

In this work, RO_2 radicals are treated as a single species, with generalised rate constants taken from the MCMv3.3.1: at 298 K and 1 atm, $k_7 = \beta \times 9.0 \times 10^{-12}$ cm^3 molecule^{-1} s^{-1}, where β is the $RONO_2$ yield which we have assumed to be a constant 5% for all RO_2 species (Orlando and Tyndall, 2012; Tan et al., 2019); $k_9 = 3.5 \times 10^{-13}$ cm^3 molecule^{-1} s^{-1}; and $k_{10} = 2.3 \times 10^{-11}$ cm^3 molecule^{-1} s^{-1}.

In line with Tan et al. (2019), we did not explicitly consider equilibrium reactions of the type $HO_2 + NO_2 \rightleftharpoons HO_2NO_2$ and $RO_2 + NO_2 \rightleftharpoons RO_2NO_2$ (e.g, peroxyacetyl nitrate (PAN) formation and decomposition) in the budget analyses, and assume these processes result in no net gain or loss of the radical species.

2.1.2 OH

OH is formed by reactions (R1), (R2), and (R4) (primary production). In addition, there are secondary OH sources from radical recycling reactions of HO_2:

$$HO_2 + NO \rightarrow OH + NO_2 \quad \text{(R11)}$$
$$HO_2 + O_3 \rightarrow OH + 2O_2 \quad \text{(R12)}$$

OH production rates are therefore given by:

$$P_{OH} = 2J(O^1D)[O_3]\,f + J(HONO)[HONO] + k_{11}[HO_2][NO] + k_{12}[HO_2][O_3] + \Sigma^i(k^i_4\,[O_3][ALK_i]Y^{OH}_{ALKi}) \quad \text{(E3)}$$

We do not consider the photolysis of hypohalous acids (HOX, e.g., HOI or HOBr) as a source of OH owing to the lack of IO or BrO measurements during ICOZA needed to quantify this. However, given the levels of NO at WAO, we expect the HOX source to only be very minor compared to reaction (R11) owing to the absence of exposed macroalgae and thus low inputs of I and Br.

OH loss rates are obtained directly from measured [OH] and measured OH reactivity:

$$D_{OH} = [OH]k'_{OH} \quad \text{(E4)}$$

2.1.3 HO_2

As shown in Section 2.1.1, primary sources of HO_2 are OVOC photolysis (of HCHO and CH_3CHO, reaction (R3)) and alkene ozonolysis (reaction (R4)). Secondary HO_2 sources are as follows:

$$OH + CO + O_2 \rightarrow HO_2 + CO_2 \quad \text{(R13)}$$

https://doi.org/10.5194/acp-2022-213
Preprint. Discussion started: 4 April 2022


Atmospheric Chemistry and Physics Discussions

$$OH + HCHO \rightarrow HO_2 + CO + H_2O \quad \text{(R14)}$$

$$RO_2 + NO \rightarrow RO + NO_2 \quad \text{(R15a)}$$

$$RO + O_2 \rightarrow R'CHO + HO_2 \quad \text{(R15b)}$$

The total HO_2 production rate may therefore be calculated as:

$$P_{HO2} = \Sigma^i(J(OVOC_i)[OVOC_i]Y^{HO2}{}_{OVOCi}) + \Sigma^j(k^j{}_4[O_3][ALK_j]Y^{HO2}{}_{ALKj}) + k_{13}[OH][CO] + k_{14}[OH][HCHO] + k_{15}[RO_2][NO]\ , \quad \text{(E5)}$$

where $k_{15} = \alpha \times 9.0 \times 10^{-12}$ cm^3 molecule^{-1} s^{-1} at 298 K (α is the HO_2 yield and equal to 0.95).

HO_2 is lost through reactions R8, R10, R11, and R12 (we do not consider the reactions of IO or BrO for reasons given in Section 2.1.2). Thus, the HO_2 destruction rate is given by:

$$D_{HO2} = (2k_8[HO_2] + k_{10}[RO_2] + k_{11}[NO] + k_{12}[O_3])[HO_2] \quad \text{(E6)}$$

2.1.4 RO_2

Analogous to HO_2, primary RO_2 sources are OVOC photolysis (of CH_3CHO and CH_3COCH_3) and alkene ozonolysis. The major secondary source of RO_2 radicals is the reaction of OH with VOCs and OVOCs:

$$OH + RH + O_2 \rightarrow RO_2 + H_2O \quad \text{(R16)}$$

The RO_2 production rate from reaction (R16) ($P^{sec.}{}_{RO2}$) may be calculated using measured VOC and OVOC concentrations, multiplied by their OH reaction rate constants and [OH] (i.e., $P^{sec.}{}_{RO2} = [OH] \times \sum^i k_{OH + VOCi}[VOC_i]$). However, given we showed that missing OH reactivity was significant in our companion paper (Woodward-Massey et al., 2022), this method would underestimate $P^{sec.}{}_{RO2}$. Alternatively, we can calculate $P^{sec.}{}_{RO2}$ from measured OH reactivity, after corrections for the contributions of inorganic reactants (i.e., NO_x, CO, SO_2, etc.) and organics that do not produce RO_2 (i.e., HCHO):

$$k'_{OH,\ corrected} = k'_{OH} - k'_{OH,\ inorganic} - k'_{OH,\ HCHO} \quad \text{(E7)}$$

$$P^{sec.}{}_{RO2} = [OH]k'_{OH,\ corrected} \quad \text{(E8)}$$

The total RO_2 production rate is then calculated as:

$$P_{RO2} = \Sigma^i(J(OVOC_i)[OVOC_i]Y^{RO2}{}_{OVOCi}) + \Sigma^j(k^j{}_4[O_3][ALK_j]Y^{RO2}{}_{ALKj}) + P^{sec.}{}_{RO2} \quad \text{(E9)}$$

https://doi.org/10.5194/acp-2022-213
Preprint. Discussion started: 4 April 2022


Atmospheric Chemistry and Physics Discussions

The reactions of the nitrate radical (NO_3) and chlorine atoms (Cl) with VOCs and OVOCs could also constitute a source of RO_2. NO_3 radical concentrations were measured during ICOZA but data coverage was poor; we have therefore omitted NO_3 radical reactions in our budget analyses. We note that this limitation should only impact the nighttime results. The impact of Cl atom chemistry is discussed in Section 3.7.

RO_2 radicals are lost through reactions (R7), (R9), (R10), and (R15). From these reactions, the total RO_2 destruction rate may be derived as:

$$D_{RO2} = ((k_7 + k_{15})[NO] + 2k_9[RO_2] + k_{10}[HO_2])[RO_2] \quad \text{(E10)}$$

3 Results

3.1 Experimental radical budget balance

3.1.1 Total RO_x

Figure 1 shows median diel profiles of the rates of RO_x production and destruction calculated using equations (E1–E2), split according to wind direction. In NW–SE air, which was encountered for ~40% of the data, both $P(RO_x)$ and $D(RO_x)$ peak at ~0.7–0.8 ppbv h^{-1} around 12:00 UTC with a fairly symmetrical profile either side of midday (solar noon ~12:00 UTC based on cloud-free days). Within uncertainty, $P(RO_x)$ and $D(RO_x)$ are equal for much of the day, indicating budget closure, apart from around midnight. In SW air (~60% of the data), $P(RO_x)$ and $D(RO_x)$ peak at ~1.2–1.4 ppbv h^{-1} around 10:00 UTC, where $D(RO_x)$ displays a broader profile than that in NW–SE air. $P(RO_x)$ is always smaller than $D(RO_x)$, by greater than the measurement uncertainty in the hours 06:00–09:00 UTC, late afternoon, and evening, suggesting missing RO_x sources in SW air on the order of ~0.2–0.6 ppbv h^{-1} at these times. Since NO_3 + VOC reactions were omitted from the budget analysis, it is suggested that NO_3 radical reactions, acting as a net RO_x source, would likely reduce the gap between $P(RO_x)$ and $D(RO_x)$ at night.

3.1.2 OH

Figure 2 displays median diel profiles of OH production and destruction calculated using equations (E3–E4). In contrast to the RO_x budget, in which production and destruction were in balance for most of the 24 h diel cycle in NW–SE air, $P(OH)$ is almost always smaller than $D(OH)$ in NW–SE air, which, since $D(OH)$ is calculated directly from measured OH reactivity, indicates missing OH sources of up to ~2–3 ppbv h^{-1}. In addition, $D(OH)$ exhibits two diel peaks at ~10:00 UTC (~2.5 ppbv h^{-1}) and ~16:00 UTC (~3.5 ppbv h^{-1}), whereas $P(OH)$ peaks only once at ~1.5 ppbv h^{-1} in the morning and then decreases through midday and over the course of the afternoon. It should be noted that the peak at ~16:00 UTC is the 1-hour median of many 15-minute data points, corresponding to different days, and is not driven by a single high value in the averaging. In SW

https://doi.org/10.5194/acp-2022-213
Preprint. Discussion started: 4 April 2022


Atmospheric Chemistry and Physics Discussions

air, OH production and destruction are reasonably well balanced throughout the day, with P(OH) slightly smaller than D(OH) by ~0.2 ppbv h^{-1} on average, but differences of up to ~1 ppbv h^{-1} (~14:00 UTC) can be seen.

3.1.3 HO_2

In contrast to the RO_x and OH budgets, the HO_2 budgets calculated using equations (E5–E6) (Figure 3) are out of balance throughout the daytime in both NW–SE and SW air, with HO_2 production greatly exceeding destruction by up to an order of magnitude in the morning. $P(HO_2)$ peaks around ~10:00 UTC at ~8 and ~14 ppbv h^{-1} in NW–SE and SW air, respectively. At this time, known HO_2 sinks amount only to ~1 ppbv h^{-1}. $D(HO_2)$ reaches diel maxima of only ~1 and ~2 ppbv h^{-1} in NW–SE and SW air, respectively. The imbalance between $P(HO_2)$ and $D(HO_2)$ cannot be accounted for by the measurement uncertainty in $D(HO_2)$ of ~44% (derived from calibration accuracy and reproducibility), and would imply the very rapid build-up of HO_2 to multi-ppbv levels, which was not observed.

3.1.4 RO_2

The diel profiles of RO_2 production and destruction calculated using equations (E7–E10) (Figure 4) bear close resemblance to those of HO_2 but with opposite sign imbalances, i.e., for RO_2, destruction greatly exceeds known production processes. In NW–SE air, $D(RO_2)$ peaks at ~7 ppbv h^{-1} around ~10:00 UTC, at which time known RO_2 sources amount to only ~0.6 ppbv h^{-1}. Maximum $P(RO_2)$ occurs around midday at almost 1 ppbv h^{-1}, which is a factor of three slower than $D(RO_2)$ at the same time. RO_2 destruction is even faster in SW air, reaching ~13 ppbv h^{-1} around 09:00–10:00 UTC, at which time $P(RO_2)$ is only ~0.6–1.5 ppbv h^{-1}. RO_2 production was almost twice as fast in SW air compared to NW–SE air, with a diel maximum of ~2 ppbv h^{-1} around ~14:00 UTC.

3.2 Dependences on NO mixing ratios

To summarise thus far, in NW–SE air during daytime the total RO_x budget is balanced but OH is missing a source, and HO_2 production rates greatly exceed HO_2 destruction rates while the opposite is true for RO_2. In SW air, evidence for missing RO_x sources is found in the morning and late afternoon, while the daytime OH budget is balanced, and the same problems with the HO_2 and RO_2 budgets in NW–SE air are also found (i.e., calculated $RO_2 \rightarrow HO_2$ conversion is perhaps too fast in both wind sectors).

In our companion paper (Woodward-Massey et al., 2022), we show that radical levels and measurement-model ratios are strongly dependent on NO mixing ratios. It is therefore expected that the budget imbalances shown in Section 3.1 of the present work may also have been influenced by NO. As shown in Figure 5, this was indeed the case, with the difference between the rate of destruction and the rate of production displaying a strong dependence on NO for RO_x, HO_2, and RO_2.

$D(RO_x) - P(RO_x)$ increases with NO in NW–SE air, from virtually zero (i.e., budget balance) at <600 pptv NO to almost 1 ppbv h^{-1} at ~2000–3000 pptv NO. This suggests missing RO_x sources and/or overestimated RO_x loss rates under high NO_x conditions. However, in SW air, the difference between destruction and production exhibits a U-shaped dependence on NO.

https://doi.org/10.5194/acp-2022-213
Preprint. Discussion started: 4 April 2022


Atmospheric Chemistry and Physics Discussions

$D(RO_x) - P(RO_x)$ is ~1 ppbv h^{-1} at ~100–200 pptv NO, scattered around zero in the ~300–600 pptv NO region, and increases again to ~0.5 ppbv h^{-1} at 1000–2000 pptv NO. This may suggest that in SW air, the radical chemistry is well-understood at moderate NO_x, but that there are missing RO_x sources and/or overestimated RO_x loss rates at both low and high NO_x. It is unclear why the budget is balanced at low NO_x in NW–SE air, but not SW air, but may relate to differences in VOC composition between the two wind sectors (Woodward-Massey et al., 2022).

For OH, the rate of destruction minus the rate of production does not exhibit any obvious trend with NO level, with values of ~0–2 ppbv h^{-1} across the entirety of NO space encountered during ICOZA, in both NW–SE and SW air. Since $D(OH)$ is constrained by measured OH reactivity, this suggests the presence of missing OH sources, which are independent of NO. One possibility is that OH radicals were formed from the reactions of HO_2 or RO_2 with species other than NO, discussed in further detail in Section 3.4. In our companion paper (Woodward-Massey et al., 2022), we present evidence for missing OH sources at low NO that are not apparent at high NO. Although this contrasts with the lack of NO-dependence found for $D(OH) - P(OH)$, their ratios $D(OH)/P(OH)$ do show a decreasing trend with NO (data not shown), consistent with the presence of missing OH sources under low NO_x conditions.

For the HO_2 and RO_2 budgets, the NO trends are the same in NW–SE and SW air. $D(HO_2) - P(HO_2)$ is close to zero at low NO, but becomes more negative with increasing NO, reaching –(12–15) ppbv h^{-1} at >1000 pptv NO. Similarly, for RO_2, the budget is closed at low NO but $D(RO_2) - P(RO_2)$ reaches up to +(13–16) ppbv h^{-1} at high NO. Thus, the HO_2 and RO_2 budget balances show virtually the same trends with NO in magnitude, but with opposite sign. This is strong evidence that the rate of $RO_2 \rightarrow HO_2$ propagation has been substantially overestimated and is discussed in further detail in Section 3.5.

3.3 Radical sources and sinks

3.3.1 RO_x initiation and termination

Figure 6 displays diel profiles of the contributions of known RO_x sources and sinks, split according to wind direction. Table 1 summarises these data by presenting the median daytime (defined as $J(O^1D) > 5 \times 10^{-7}$) percentage contributions of individual RO_x sources and sinks in NW–SE and SW air. In NW–SE air, RO_x initiation had roughly equal contributions from $O^1D + H_2O$ and HONO photolysis (~37%) on average, where HONO photolysis dominated RO_x initiation in the early morning (~05:00–08:00 UTC) but was less important over the rest of the day. In contrast, HONO photolysis was dominant (median 44% vs 29% for $O^1D + H_2O$) in the more polluted SW air (Woodward-Massey et al., 2022) throughout the day. This might be expected based on the mixing ratios of HONO in each wind sector type, with median values of 52 and 97 pptv in NW–SE and SW air, respectively. The contributions from carbonyl (HCHO, acetaldehyde, and acetone) photolysis (~23–25%) and ozonolysis (~3%) were about the same in each wind sector type.

In terms of RO_x termination, the main contributors in both wind sector types were calculated to be alkyl nitrate formation, $RO_2 + HO_2$ reactions, and the reaction of OH with NO_2 to yield HNO_3. In NW–SE air, these three loss processes were of equal importance on average (~30%), with alkyl nitrate formation dominant around ~09:00 UTC and $RO_2 + HO_2$ reactions dominant

https://doi.org/10.5194/acp-2022-213
Preprint. Discussion started: 4 April 2022


Atmospheric Chemistry and Physics Discussions

in the afternoon. The contributions from HO_2 + HO_2, RO_2 + RO_2, and OH + NO were all small on average (<4%). The contributions from alkyl nitrate and HNO_3 formation were greater in SW air (almost 40% on average), whereas RO_2 + HO_2 reactions were less important (~14%), driven by differences in NO_x levels between the two wind sectors. Again, alkyl nitrate formation was most important in the morning, but also contributed substantially throughout the afternoon. HO_2 + HO_2 and RO_2 + RO_2 reactions were almost negligible (~1%), but the contribution from OH + NO (~6%) was greater than in NW–SE air (~3%).

3.3.2 OH production and k'_{OH}

The breakdown of OH production and its comparison to measured OH destruction ([OH] × k'_{OH}) is given in Figure 7, again split by wind direction. These data are summarised in Table 2, which shows the median daytime contributions of the known OH sources. Similarly, Figure 8 gives the breakdown of OH reactivity and comparison to measured k'_{OH}, also summarised in Table 2.

OH production was dominated throughout the daytime by the secondary source HO_2 + NO in both NW–SE (~50% on average) and SW (~70%) air. In NW–SE air, the next most important OH sources were the primary sources O^1D + H_2O and HONO photolysis, with average contributions of ~23% each. Similar to the RO_x budget (Section 3.3.1), HONO photolysis (~18%) was more important than O^1D + H_2O (~12%) as an OH source in the more polluted SW air. Radical recycling from HO_2 + O_3 (<3%) and radical initiation from ozonolysis (<1%) were of only minor importance in both wind sector types.

In terms of OH loss (Table 2), the most important OH reactant was CO (NW–SE daytime median: ~42% of calculated OH reactivity, SW: ~27%), followed by NO_2 (~20%, ~26%), reflecting the overall dominance of inorganic reactants to calculated OH reactivity. In terms of organic OH reactivity, carbonyls (~13%, ~21%; mostly (~57%) HCHO) and alkenes and alkynes (~6–8%; mostly (~62%) propene) were the most important species. The dialkenes isoprene and 1,3-butadiene made small but significant contributions to OH reactivity (~4–6%), whereas the contributions from aromatics, alkanes, and methanol were all minor (≤3%). Missing OH reactivity was similar in magnitude in both wind sectors (~50%). Monoterpenes (MTs) were not included in the calculation of OH reactivity as their sum (measured using proton transfer reaction–mass spectrometry, PTR–MS) was generally below the LOD; if we use these data, the maximum contribution of MTs was only ~0.4 s^{-1} (median 0.04 s^{-1}, compared to measured k'_{OH} ~ 4.7 s^{-1}), using the rate constant for OH + limonene.

3.4 Attempting to balance the radical budgets

In this section, we describe various attempts to try and balance the radical budgets through making modifications to the calculation of experimental budgets. Such modifications include: (1) the addition of generic radical recycling processes, (2) reduction of the rate of RO_2 → HO_2 conversion, (3) inclusion of heterogeneous HO_2 uptake, and (4) addition of chlorine chemistry.

https://doi.org/10.5194/acp-2022-213
Preprint. Discussion started: 4 April 2022


Atmospheric Chemistry and Physics Discussions

3.4.1 OH from RO_2 + X and HO_2 + Y

The artificial species "X" has previously been invoked as a candidate to account for missing OH sources (Hofzumahaus et al., 2009; Whalley et al., 2011; Lu et al., 2012; Lu et al., 2013; Rohrer et al., 2014; Tan et al., 2017; Tan et al., 2019). Here, X is a species that acts like NO, reacts with the same rate constant as NO, and yields an additional secondary source of OH from RO_2 and HO_2:

$$RO_2 + X \rightarrow HO_2 \quad \text{(R17)}$$

$$HO_2 + X \rightarrow OH \quad \text{(R18)}$$

However, unlike the analogous process for NO, reactions (R17–R18) do not result in the concomitant production of NO_2 and hence ozone (reactions (R11) and (R15a)). Similarly, direct conversion of HO_2 to OH using another artificial species "Y", which does not react with RO_2 radicals, was proposed by (Lu et al., 2012; Lu et al., 2013):

$$HO_2 + Y \rightarrow OH \quad \text{(R19)}$$

In the present work, we have applied these two generic recycling mechanisms from species X and Y to test whether they are able to close the OH budget, using measured HO_2 and RO_2. Note that here, we have treated reactions (R17–R18) as a one step process in which RO_2 is directly converted to OH by X (i.e., $RO_2 + X \rightarrow OH$). We have assumed the same rate constants for the reactions of X/Y with RO_2/HO_2 as for NO, and set the abundance of each hypothetical species X and Y to a constant 100 pptv, a value used in a previous study in the North China Plain (Tan et al., 2017). These results are displayed in Figure 9. It can be seen that P(OH) is increased significantly after the incorporation of both the X and Y mechanisms. In NW–SE air, the X mechanism results in P(OH) being greater than D(OH) during nighttime and for much of the daytime, with the exception of ~09:00 UTC and ~16:00 UTC. The Y mechanism results in much more modest increases in P(OH), due to lower observed HO_2 concentrations (Woodward-Massey et al., 2022). Neither mechanism is able to balance the OH budget, especially the afternoon peak in D(OH). However, it is likely that assumptions about the mixing ratios of X and Y are not correct, or that the assumption of constant concentrations is invalid. In SW air, the X mechanism again results in P(OH) being greater than D(OH) during nighttime and for most of the daytime. However, the Y mechanism results in reasonable balance between P(OH) and D(OH), apart from around 06:00 UTC when HO_2 concentrations were lower. In both NW–SE and SW air, the X mechanism slightly improves the agreement between $P(HO_2)$ and $D(HO_2)$, but slightly worsens the agreement between $P(RO_2)$ and $D(RO_2)$; however, the changes are small overall compared with the imbalances in both HO_2 and RO_2 budgets.

3.4.2 $HO_2 + Z \rightarrow RO_2$

Considering that during the daytime, $P(HO_2) \gg D(HO_2)$ and $P(RO_2) \ll D(RO_2)$ simultaneously, it is possible that there is an unknown species "Z" that is able to recycle HO_2 back to RO_2:

$$HO_2 + Z \rightarrow RO_2 \quad \text{(R20)}$$

A candidate for species Z may be a carbonyl containing compound, which are known to undergo (reversible) HO_2 addition. For example, HO_2 has been shown to add to formaldehyde (Veyret et al., 1989), acetaldehyde (Tomas et al., 2001), acetone

https://doi.org/10.5194/acp-2022-213
Preprint. Discussion started: 4 April 2022


Atmospheric Chemistry and Physics Discussions

(Grieman et al., 2011), and methylglyoxal (Orlando and Tyndall, 2020) experimentally, and equilibria of this type have been investigated theoretically (Niki et al., 1985; Hermans et al., 2005). These reactions have generally been shown to have negligible impacts on atmospheric chemistry, but it can be speculated that a higher order or more functionalised carbonyl compound may add HO_2 to form a much more strongly bound complex.

Regardless of the identity of species Z, such a mechanism is able to simultaneously reduce the HO_2 and RO_2 budget imbalances, as shown in Figure 10. Assuming a constant mixing ratio of 500 pptv and similar reactivity to NO, the Z mechanism is able to close the HO_2 and RO_2 budgets in the afternoon, but does not perturb the OH budget. Morning imbalances are still present, but this may be because the assumption of constant Z concentrations is invalid and that Z levels were higher in the morning.

3.4.3 Reducing the rate of $RO_2 \rightarrow HO_2$ conversion

(Whalley et al., 2018) presented field measurements of HO_2 and RO_2 radicals in London. HO_2 levels were significantly overpredicted by an MCM model during the daytime, particularly in air that had passed over central London. It was found that HO_2 concentrations could be reasonably well simulated if the fraction of RO_2 radicals that propagated to HO_2 (i.e., the branching ratio α in reactions (R7) and (R15a)) was reduced. To achieve good agreement, α was reduced to 0.15, compared to $\alpha \sim 0.5$ in the base model, a factor of ~3 reduction.

In the present work, α was set to 0.95 based on literature values of the branching ratios for alkyl nitrate formation (β) of ~5% (Orlando and Tyndall, 2012; Tan et al., 2019). However, even with such a low $RONO_2$ branching ratio, $P(RONO_2)$ values of up to ~0.7 ppbv h^{-1} (Figure 6) are already very high considering previous measurements of $RONO_2$ at Weybourne were on the order of tens of pptv (Worton et al., 2010). Therefore, it is not thought that changing the value of α is appropriate for ICOZA. Instead, we have artificially reduced the rate of $RO_2 \rightarrow HO_2$ conversion by changing the total rate constant of reactions (R7) and (R15a) (originally 9.0×10^{-12} cm^3 $molecule^{-1}$ s^{-1} at 298 K). The impact of reducing the RO_2 + NO rate constant by a factor of 5 on the HO_2 and RO_2 budgets is shown in Figure 11. It can be seen that the HO_2 and RO_2 budgets are now reasonably well balanced in the afternoon, but still $P(HO_2) > D(HO_2)$ and $P(RO_2) < D(RO_2)$ by ~1–2 ppbv h^{-1} in the morning. It should be noted that no evidence exists for such low RO_2 + NO rate constants, with published k(298 K) values in the range ~8–20 $\times 10^{-12}$ cm^3 $molecule^{-1}$ s^{-1} and associated uncertainties of ~15–35% (Orlando and Tyndall, 2012), although the kinetics of relatively few RO_2 species with NO have been studied directly.

3.4.4 Inclusion of heterogeneous HO_2 uptake

Up to now, the heterogeneous uptake of HO_2 has not been considered in the HO_2 budget, although it was included in the MCM models in our companion paper (Woodward-Massey et al., 2022). We have assessed the impact of this chemistry on the experimental HO_2 budget in Figure 12. The heterogeneous loss of HO_2 was parametrised using the following first-order loss rate (Ravishankara, 1997):

https://doi.org/10.5194/acp-2022-213
Preprint. Discussion started: 4 April 2022


Atmospheric Chemistry and Physics Discussions

$$k'_{loss} = \omega A \gamma / 4 \,, \quad \text{(E11)}$$

where ω is the mean molecular speed of HO_2 (43725 cm s^{-1} at 298 K), A is the aerosol surface area measured by the aerodynamic particle sizer (APS), and γ is the aerosol uptake coefficient.

Using γ = 0.1, a value consistent with previous laboratory experiments (Mozurkewich et al., 1987; George et al., 2013; Lakey, 2014; Lakey et al., 2015; Lakey et al., 2016; Moon, 2018) and the same value used in the MCM model in our companion paper (Woodward-Massey et al., 2022), the impact on the HO_2 budget is negligible. Even increasing γ to unity has virtually no effect on $D(HO_2)$, due to the low particulate matter loading observed during ICOZA (A ~ 0.6–4.2 × 10^{-7} cm^2 cm^{-3}).

3.4.5 Inclusion of chlorine chemistry

A missing primary RO_2 source has been invoked previously to help explain model underpredictions of RO_2 (Tan et al., 2017) in which it was hypothesised that reactions of chlorine atoms (e.g., from the photolysis of Cl_2 or $ClNO_2$ (Osthoff et al., 2008)) with VOCs during the morning were the source of the missing RO_2, although the contribution was not sufficient to explain the magnitude of the RO_2 underprediction (inclusion of Cl chemistry accounted for only ~10–20% of the missing RO_2).

Cl_2 and $ClNO_2$ were both measured during ICOZA (Sommariva et al., 2018), such that their impact on the RO_2 budget can be assessed. Assuming that all photolysed Cl atoms react with VOCs, rather than with inorganic species, i.e., $P(\text{Cl-RO}_2) \approx P(\text{Cl}) = 2J(\text{Cl}_2)[\text{Cl}_2] + J(\text{ClNO}_2)[\text{ClNO}_2]$, an upper limit of the impact of chlorine chemistry can be derived. Figure 13 shows that even this upper limit contribution has negligible impacts on the RO_2 budget, ruling out chlorine chemistry as the source of the RO_2 budget discrepancy. In NW–SE air, the upper limit contribution from chlorine chemistry ($P(\text{Cl-RO}_2)$) peaked in the morning at ~0.08 ppbv h^{-1}, but peaked in the afternoon in SW air at ~0.12 ppbv h^{-1}, in comparison to $P(RO_2)$ and $D(RO_2)$ values of up to ~2 and ~14 ppbv h^{-1}, respectively These results are consistent with a previous report of the small impact of chlorine oxidation at the WAO (Bannan et al., 2017).

3.5 Ozone production

3.5.1 Calculated $P(O_x)$ and comparison to MCM model predictions

The gross *in situ* ozone production rate, $p(O_3)$, may be defined in terms of the rate of net NO → NO_2 conversion (Cazorla et al., 2012), i.e., $p(O_x)$ where $O_x = O_3 + NO_2$:

$$p(O_3) \approx p(O_x) = k_{11}[HO_2][NO] + k_{RO2+NO}[RO_2][NO] \times \alpha \quad \text{(E12)}$$

Here, α is the branching ratio for $HO_2 + NO_2$ formation (reaction (R15)) and k_{RO2+NO} is the total rate constant for reactions (R7) and (R15). The chemical loss rate of ozone, $l(O_3)$, may be derived from the rate of radical-NO_x termination reactions and the loss of O_3 to HO_2, approximated by:

https://doi.org/10.5194/acp-2022-213
Preprint. Discussion started: 4 April 2022

Atmospheric Chemistry and Physics Discussions

$$l(O_3) \approx l(O_x) = k_6[OH][NO_2][M] + k_{RO2+NO}[RO_2][NO] \times \beta + k_{12}[HO_2][O_3] \,, \quad \text{(E13)}$$

where β (= 1 – α) is the branching ratio for $RONO_2$ formation (reaction (R7)). The net ozone production rate, $P(O_3)$, is then obtained from the difference between equations (E13) and (E14):

$$P(O_3) \approx P(O_x) = p(O_x) - l(O_x) \quad \text{(E14)}$$

Calculation of $P(O_3)$ ($\approx P(O_x)$) from FAGE observations of HO_2 and RO_2 radicals was one of the main aims of the ICOZA project.

Median diel profiles of the net ozone production, $P(O_x)$, calculated from measured and modelled (Woodward-Massey et al., 2022) OH, HO_2, and RO_2 radical concentrations are shown in Figure 14. Here, $P(O_x)$ was calculated from equations (E12–E14) with the same values of k_{RO2+NO} and α (= 0.95) applied to both observations and model predicted concentrations of total RO_2 (i.e., model $P(O_x)$ was not calculated from the rate constants and yields for individual RO_2 species). k_{RO2+NO} was set to the generic value used in the MCM (k_{RO2+NO} = 2.7 × 10^{-12} exp(360/T) = 9.0 × 10^{-12} cm^3 $molecule^{-1}$ s^{-1} at 298 K; for reference, $k_{CH3O2+NO}$ = 7.7 × 10^{-12} cm^3 $molecule^{-1}$ s^{-1} at 298 K).

In NW–SE air, FAGE-calculated $P(O_x)$ peaks at ~16 ppbv h^{-1} at 09:30 UTC when NO and peroxy radical levels are both high (Woodward-Massey et al., 2022), before decreasing sharply in the afternoon to ~0.7–1.4 ppbv h^{-1}. Model-calculated $P(O_x)$ also peaks at 09:30 UTC but at a ten-fold lower value of ~1.6 ppbv h^{-1}. The afternoon decrease is less severe than for FAGE-calculated $P(O_x)$, resulting in good agreement between FAGE- and model-calculated $P(O_x)$ in the afternoon. In SW air, FAGE-calculated $P(O_x)$ displays a broader morning peak in the hours ~07:00–10:00 UTC of ~10–15 ppbv h^{-1}. In comparison to NW–SE air, afternoon FAGE-calculated $P(O_x)$ was greater with values of ~5–8 ppbv h^{-1}. Daytime model-calculated $P(O_x)$ is in the range 0.3–2.3 ppbv h^{-1}, peaking at 14:30 UTC, and underpredicts the observations throughout the daytime, in contrast to NW–SE air.

3.5.2 Ozone production regime – L_n / Q

The ratio of the rates of radical loss to NO_x (L_n, reactions (R5–R7)) to total radical initiation ($Q = P(RO_x) \approx D(RO_x)$) has been proposed as a simple metric to assess whether ozone production is NO_x or VOC limited (Kleinman et al., 1997; Kleinman et al., 2001). A ratio above 0.5 suggests that ozone production is VOC limited, while values below 0.5 indicate that ozone production is in the NO_x limited regime. This metric has been used to assess ozone production sensitivity in previous urban campaigns (Mao et al., 2010; Griffith et al., 2016).

In the present work, calculated $D(RO_x)$ was generally slightly greater than $P(RO_x)$ (Figure 1) and calculated L_n often exceeded $P(RO_x)$, leading to L_n / Q ratios of greater than 1. For this reason, we have used the ratio of radical loss to NO_x to total radical destruction (L_n / $D(RO_x)$) to assess ozone production sensitivity for the ICOZA campaign. Median diel profiles of

https://doi.org/10.5194/acp-2022-213
Preprint. Discussion started: 4 April 2022


Atmospheric Chemistry and Physics Discussions

daytime (06:00–21:00 UTC) L_n / $D(RO_x)$ calculated from measured radicals in NW–SE and SW air are shown in Figure 15. In NW–SE air, ozone production was generally VOC limited (i.e., L_n / $D(RO_x)$ > 0.5), but with some NO_x limited ozone production around midday. In contrast, ozone production was VOC limited throughout the daytime in the more polluted SW air.

3.5.3 $P(O_x)$ dependence on NO mixing ratios

Considering the strong dependence of measured and modelled HO_2 and RO_2 radical concentrations on NO mixing ratios (Woodward-Massey et al., 2022), it is expected that $P(O_x)$ should also exhibit a NO-dependence. Figure 16 shows that both FAGE- and model-calculated $P(O_x)$ are strongly dependent on NO, with similar trends in NW–SE and SW air. FAGE-calculated $P(O_x)$ shows a consistent increase with NO in both NW–SE and SW air, with values of <1 ppbv h^{-1} below 100 pptv NO and up to ~17 ppbv h^{-1} at ~2–3 ppbv NO. In contrast, model-calculated $P(O_x)$ starts to fall off a little above 1 ppbv NO in NW–SE air, but generally increases with NO in SW air. Below ~500 pptv NO, FAGE- and model-calculated $P(O_x)$ are in reasonable agreement within combined uncertainties. However, above this threshold, FAGE-calculated $P(O_x)$ is much greater than model-calculated $P(O_x)$, with measurement-to-model ratios of up to ~5–15 for NO ~2–3 ppbv. NO_x levels were not high enough to show any onset of a plateau in FAGE-calculated $P(O_x)$.

4 Discussion

Overall, the results show that during the daytime, the budget of total RO_x is virtually closed in both wind sectors (Figure 1), although there is evidence for relatively small missing RO_x sources in the early morning and late afternoon in SW air. However, the budgets for individual RO_x species are out of balance, most severely for HO_2 (Figure 3) and RO_2 (Figure 4). The dependence of these imbalances on NO_x levels (Figure 5) implies that there are quantitative limitations to our understanding of the processes that interconvert RO_x species, in particular those that convert RO_2 to HO_2. The worst agreement between experimental HO_2 and RO_2 production and destruction rates is found at high NO_x, suggesting that it is under these conditions that our understanding is most incomplete.

Various hypotheses were tested to see whether we could achieve budget closure for individual RO_x species. First, it was assessed whether additional unknown recycling processes that convert HO_2 (+ Y) or RO_2 (+ X) to OH could reduce the budget imbalances for OH, HO_2, and RO_2. Under this hypothesis, there was some improvement to the agreement between OH production and destruction, but budget balance could not be achieved for all three species simultaneously (Figure 9).

Second, another unknown species Z that facilitates the conversion of HO_2 to RO_2 was suggested. Incorporation of this mechanism did simultaneously reduce the budget imbalances for HO_2 and RO_2 (Figure 10), without affecting the OH budget. However, it is not clear what the identity of species Z could be, or at what concentration it may exist in the atmosphere, but certainly this candidate mechanism warrants further research.

https://doi.org/10.5194/acp-2022-213
Preprint. Discussion started: 4 April 2022


Atmospheric Chemistry and Physics Discussions

Third, the RO_2 + NO rate constant was reduced to assess the impact on experimental HO_2 and RO_2 budgets. Of all the hypotheses tested in the present work, this resulted in the best agreement between HO_2 and RO_2 production and destruction rates (Figure 11). However, the RO_2 + NO rate constant had to be reduced by a factor of 5 to achieve this, for which no evidence exists, given that accepted laboratory measurements of these rate constants for specific peroxy species have not reported values as low and have uncertainties in the range ~15–35% (Orlando and Tyndall, 2012). It is therefore imperative that more laboratory studies are conducted to measure RO_2 + NO rate constants with a wide variety of RO_2 types. Given that organic OH reactivity was dominated by OVOCs and alkenes and alkynes (Table 2), it is perhaps here where efforts should focus. On the other hand, missing OH reactivity is also significant and it is unclear what species are responsible, although in our companion paper (Woodward-Massey et al., 2022) we show that the missing reactivity may be due to unmeasured OVOCs rather than BVOCs. Alternatively, previous experiments at the WAO have suggested that a multitude of aromatic species may be responsible for missing OH reactivity (Lee et al., 2009). We do note however, that different RO_2 species have different NO rate constants, while in this work we were only able to treat RO_2 radicals as a single species with a single NO rate constant, which introduces a bias in our analyses. Reduced RO_2 + NO rate constants could help to reconcile measurement-model discrepancies seen for RO_2 at high NO in other campaigns (Tan et al., 2017; Tan et al., 2018; Whalley et al., 2018; Slater et al., 2020). In addition, the reduced rate constants would result in longer RO_2 lifetimes with respect to NO. This has implications for autoxidation chemistry (Bianchi et al., 2019): longer RO_2 lifetimes would allow more time for unimolecular autoxidation reactions to compete with the bimolecular NO reaction, resulting in more efficient formation of highly-oxidised molecules (HOMs) under high NO_x conditions. This may help to explain the lack of (complete) suppression of HOM signals at higher NO_x seen in some laboratory experiments (e.g., Zhao et al. (2018); Mehra et al. (2020)). However, the only rate constant for a highly-oxidised RO_2 radical with NO that has been measured (Berndt et al., 2015) was found to be ~3–4 times faster than the rate constant used in the present work.

Finally, it was assessed whether HO_2 heterogeneous uptake or chlorine chemistry could reconcile the budget imbalances for HO_2 and RO_2, respectively. In both cases, the impacts on calculated production and destruction rates were negligible, thus ruling them out as the sources of the budget discrepancies.

The simultaneous measurement of RO_x, NO, and NO_2 allowed for the calculation of *in situ* ozone production rates (Figure 14). Using FAGE-measured radicals, daily integrated (06:00–21:00 UTC) ozone productions of 38 and 80 ppbv in NW–SE and SW air, respectively, were calculated. The daily integrated ozone productions calculated from MCM-modelled radicals are much lower at 9 and 15 ppbv, respectively. These values may be compared to those calculated from measured ozone at 18 and 20 ppbv, respectively. The large difference between FAGE-calculated ozone production and that calculated from measured ozone suggests that most of the ozone produced *in situ* was transported downwind of the WAO site. Daytime ozone production was shown to be close to the transition between NO_x-limited and VOC-limited regimes in NW–SE air, which may be considered representative of the background conditions of northern Europe. Ozone production was generally VOC-limited in the more polluted SW air, although still relatively close to the transition point (Figure 15). It was also shown that FAGE-calculated ozone production rates scaled with NO in both wind sectors (Figure 16). Taken together, these results suggest that

https://doi.org/10.5194/acp-2022-213
Preprint. Discussion started: 4 April 2022


Atmospheric Chemistry and Physics Discussions

both NO_x and VOC emissions reductions in source regions (e.g., London, Birmingham) would help to mitigate ozone pollution at this UK coastal receptor site.

The results of our work may be compared to those of Tan et al. (2019), who first used the experimental budget approach for a campaign in the Pearl River Delta (PRD), China. Pollution levels were much higher during the PRD campaign compared to those encountered at the WAO – for example much greater OH reactivities of up to 80 s^{-1} were measured (c.f. 18 s^{-1} for ICOZA), and NO mixing ratios were higher (diurnal maximum of ~4 ppbv vs ~0.8–1.4 ppbv for ICOZA). Despite this, measured radical concentrations were fairly similar, with maximum diel median concentrations of 4.5×10^6 molecule cm^{-3} for OH (c.f. 2–4 $\times 10^6$ molecule cm^{-3} during ICOZA), 3×10^8 molecule cm^{-3} for HO_2 (c.f. 1–1.5 $\times 10^8$ molecule cm^{-3}), and 2×10^8 molecule cm^{-3} for RO_2 (c.f. ~5 $\times 10^8$ molecule cm^{-3}). In the PRD, maximum loss rates for OH, HO_2, and RO_2 reached up to 10–15 ppbv h^{-1}, similar to the loss rates observed for RO_2 in SW air during ICOZA (Figure 4). The loss rate of total RO_x peaked at midday at ~3 ppbv h^{-1}, compared with ~0.8–1.2 ppbv h^{-1} for ICOZA (Figure 1), where the difference is likely due to the higher pollution levels found in the PRD (i.e., increased radical loss to NO_x). Within experimental uncertainties, the RO_x budget was balanced, similar to that observed for ICOZA. Evidence for a missing afternoon OH source was presented (with an inferred source strength of 4–6 ppbv h^{-1}), which was also the case for NW–SE air during ICOZA (up to ~2 ppbv h^{-1}, Figure 2). However, in the PRD, the HO_2 budget was closed within experimental uncertainty, and the closure of the RO_2 budget could be greatly improved when RO_2 production was calculated from measured OH reactivity, although a missing afternoon RO_2 sink was still present. This is in contrast to our results, from which a significant missing HO_2 sink (Figure 3) and a missing RO_2 source (Figure 4) on the order of 10 ppbv h^{-1} may be inferred. In the PRD, the strongest differences between calculated RO_2 production and destruction rates were found at low NO (<1 ppbv), with budget closure at high NO. However, during ICOZA, the difference between RO_2 (and HO_2) production and destruction rates was most severe at high NO (Figure 5).

More recently, Whalley et al. (2020) also assessed the experimental radical budget for RO_x and OH reactivity observations made in summertime Beijing. A missing OH source was identified under the low NO (<0.5 ppbv) conditions experienced in the afternoon, similar to that for ICOZA NW–SE air, but with a much higher inferred source strength on the order of ~15 ppbv h^{-1}. Identical to ICOZA, their budget analysis indicated that the HO_2 and RO_2 budgets were both out of balance but with opposite sign, where the ratios of production to destruction rates displayed a strong dependence on NO concentration; under the highest NO (~100 ppbv) conditions, $P(HO_2)$ exceeded $D(HO_2)$ by ~50 ppbv h^{-1} (cf. ~10–15 ppbv h^{-1} for ICOZA at ~2 ppbv NO), whilst $D(RO_2)$ exceeded $P(RO_2)$ by the same magnitude. The agreement between experimental production and destruction rates for HO_2 and RO_2 was much improved after reducing the rate of $RO_2 \rightarrow HO_2$ propagation (by reducing α from 0.95 to 0.10), similar to our approach of reducing the RO_2 + NO rate constant (Figure 11). As discussed in our companion paper (Woodward-Massey et al., 2022), Whalley et al. (2020) suggested that some complex RO_2 species (e.g., from BVOC or aromatic VOC oxidation) do not directly generate HO_2 after reaction with NO, but instead the RO radicals formed autoxidise (via H-shifts) to form new RO_2 species that undergo further reaction with NO before eventually forming HO_2. This type of chemistry serves to reduce the rate of $RO_2 \rightarrow HO_2$ propagation and could help to explain the differences between experimental production and destruction rates of HO_2 and RO_2 found for ICOZA.

https://doi.org/10.5194/acp-2022-213
Preprint. Discussion started: 4 April 2022


Atmospheric Chemistry and Physics Discussions

5 Conclusions

In our companion paper (Woodward-Massey et al., 2022), we presented measurements of radical species and k'_{OH} made during the 2015 ICOZA field campaign that took place at a coastal site in North Norfolk, UK. In the present work, the simultaneous measurement of OH, HO_2, RO_2, and k'_{OH} allowed for experimental (i.e., observationally determined) budgets to be derived for all radical species as well as total RO_x. Data were separated according to wind direction: SW winds (180°–270°), and all other winds (NW–SE, <165° and >285°). In NW–SE air, the RO_x budget could be closed during the daytime within experimental uncertainty but OH destruction exceeded OH production by ~2–3 ppbv h^{-1}, and HO_2 production greatly exceeded HO_2 destruction while the opposite was true for RO_2. In SW air, the RO_x budget analysis indicated missing daytime RO_x sources on the order of ~0.2–0.6 ppbv h^{-1} but the OH budget was balanced, and the same behaviour was found with the HO_2 and RO_2 budgets as in NW–SE air. Differences between radical destruction and production rates were found to exhibit species-dependent trends with respect to NO mixing ratios; the budget imbalances were most severe for HO_2 and RO_2 at high NO (> 1000 pptv), with differences of –(12–15) ppbv h^{-1} and +(13–16) ppbv h^{-1}, respectively.

In NW–SE air, the dominant daytime RO_x sources were $O^1D + H_2O$ and HONO photolysis (~37% each) with significant contributions from carbonyl photolysis (~23%), while the major RO_x sinks were the reactions $RO_2 + NO \rightarrow RONO_2$ (~28%), $RO_2 + HO_2$ (~33%), and $OH + NO_2$ (~33%). The major OH source was the secondary source $HO_2 + NO$ (~50%) with significant contributions from $O^1D + H_2O$ and HONO photolysis (~23% each), while in terms of OH loss, the most important reactions were OH + CO (~42%) and $OH + NO_2$ (~20%). In the more polluted SW air, RO_x initiation was dominated by HONO photolysis (~44%) with similar contributions from $O^1D + H_2O$ (~29%) and carbonyl photolysis (~25%), while RO_x termination was mainly controlled by the reactions $RO_2 + NO \rightarrow RONO_2$ (~38%) and $OH + NO_2$ (~39%). OH production was dominated by $HO_2 + NO$ (~70%), while OH loss was controlled by reactions with CO (~27%), NO_2 (~26%), and carbonyls (~21%).

After finding that the radical budgets were out of balance, most severely for HO_2 and RO_2, several modifications were made to the calculation of experimental budgets to try and reconcile this: (1) the addition of generic radical recycling processes, (2) reduction of the rate of $RO_2 \rightarrow HO_2$ conversion, (3) inclusion of heterogeneous HO_2 uptake, and (4) addition of chlorine chemistry. The best agreement between HO_2 and RO_2 production and destruction was found for (2), in which we reduced the $RO_2 + NO$ rate constant by a factor of 5. It is therefore recommended that more studies are conducted to measure $RO_2 + NO$ rate constants, in particular for more complex, functionalised RO_2.

The rate of *in situ* ozone production ($P(O_x)$) was calculated from observations of RO_x, NO, and NO_2 and compared to that calculated from MCM-modelled radical concentrations. The MCM-calculated $P(O_x)$ significantly underpredicted the measurement-calculated $P(O_x)$ in the morning by up to a factor of 10, and the degree of underprediction was found to scale with NO. Using the ratio of the rates of radical loss to NO_x to total radical loss (L_n / $D(RO_x)$), it was shown that in NW–SE air, daytime ozone production was close to the transition between NO_x-limited and VOC-limited regimes. However, in the more polluted SW air, ozone production was generally VOC-limited.

https://doi.org/10.5194/acp-2022-213
Preprint. Discussion started: 4 April 2022


Atmospheric Chemistry and Physics Discussions

The strong NO-dependences of the HO_2 and RO_2 budget imbalances reveal a systematic limitation to our understanding of peroxy radical cycling chemistry, which directly impacts our ability to calculate ozone production rates correctly. Future tropospheric ozone abatement strategies rely on the accurate simulation of ozone chemistry. It is therefore crucial that further studies seek to explain the budget imbalances found in this work.

Data availability

The data used in this study are available from the corresponding authors upon request (l.k.whalley@leeds.ac.uk and d.e.heard@leeds.ac.uk) and are also archived on CEDA (https://archive.ceda.ac.uk/).

Author contributions

WJB was the principal investigator of the ICOZA project and was responsible for organisation of the Weybourne field intensive. RWM, LKW, DRC, TI, and DEH were responsible for measurements of radicals, OH reactivity, HCHO, and photolysis frequencies (*J* values also provided by RS, SMB, and PSM). LRC, LJK, and WJB made measurements of HONO and aerosol surface area. RS, SMB, and PSM provided Cl_2 and $ClNO_2$ data. JL and CR measured NO, NO_2, and HONO. BJB was responsible for the long-term operation of the Weybourne Atmospheric Observatory and provided O_3, CO, and HCHO data. GLF was responsible for measurements of VOCs. RS conducted the MCM model simulations. RWM, LKW, and RS analysed the data. RWM wrote the manuscript with input from all co-authors.

Acknowledgements

We thank the science team of the ICOZA project. RWM and DRC are grateful to the NERC for funding PhD studentships. RWM, LKW, DRC, TI, and DEH would like to thank the University of Leeds electronic and mechanical workshops. RWM is grateful to Hans Osthoff (University of Calgary) for the provision of Igor functions, and to Chunxiang Ye (Peking University) and Samuel Seldon (University Of Leeds) for useful discussions. We thank Lloyd Hollis and Roland Leigh (University of Leicester) for assistance with the spectral radiometer and chemical ionization mass spectrometer. We thank Sam Cox for his help with the AtChem modelling framework.

Financial support

This research has been supported by the NERC (grant nos. NE/K012029/1, NE/K012169/1, and NE/K004069/1).

https://doi.org/10.5194/acp-2022-213
Preprint. Discussion started: 4 April 2022

References

Bannan, T. J., Bacak, A., Le Breton, M., Flynn, M., Ouyang, B., McLeod, M., Jones, R., Malkin, T. L., Whalley, L. K., Heard, D. E., Bandy, B., Khan, M. A. H., Shallcross, D. E., and Percival, C. J.: Ground and Airborne U.K. Measurements of Nitryl Chloride: An Investigation of the Role of Cl Atom Oxidation at Weybourne Atmospheric Observatory, Journal of Geophysical Research: Atmospheres, 122, 11,154-111,165, 10.1002/2017jd026624, 2017.

Berndt, T., Richters, S., Kaethner, R., Voigtländer, J., Stratmann, F., Sipilä, M., Kulmala, M., and Herrmann, H.: Gas-Phase Ozonolysis of Cycloalkenes: Formation of Highly Oxidized RO2 Radicals and Their Reactions with NO, NO2, SO2, and Other RO2 Radicals, The Journal of Physical Chemistry A, 119, 10336-10348, 10.1021/acs.jpca.5b07295, 2015.

Bianchi, F., Kurtén, T., Riva, M., Mohr, C., Rissanen, M. P., Roldin, P., Berndt, T., Crounse, J. D., Wennberg, P. O., Mentel, T. F., Wildt, J., Junninen, H., Jokinen, T., Kulmala, M., Worsnop, D. R., Thornton, J. A., Donahue, N., Kjaergaard, H. G., and Ehn, M.: Highly Oxygenated Organic Molecules (HOM) from Gas-Phase Autoxidation Involving Peroxy Radicals: A Key Contributor to Atmospheric Aerosol, Chemical Reviews, 119, 3472-3509, 10.1021/acs.chemrev.8b00395, 2019.

Bohn, B., Corlett, G. K., Gillmann, M., Sanghavi, S., Stange, G., Tensing, E., Vrekoussis, M., Bloss, W. J., Clapp, L. J., Kortner, M., Dorn, H. P., Monks, P. S., Platt, U., Plass-Dulmer, C., Mihalopoulos, N., Heard, D. E., Clemitshaw, K. C., Meixner, F. X., Prevot, A. S. H., and Schmitt, R.: Photolysis frequency measurement techniques: results of a comparison within the ACCENT project, Atmos Chem Phys, 8, 5373-5391, DOI 10.5194/acp-8-5373-2008, 2008.

Bohn, B., Heard, D. E., Mihalopoulos, N., Plass-Dülmer, C., Schmitt, R., and Whalley, L. K.: Characterisation and improvement of <i>j</i>(O¹D) filter radiometers, Atmos Meas Tech, 9, 3455-3466, 10.5194/amt-9-3455-2016, 2016.

Brune, W. H., Baier, B. C., Thomas, J., Ren, X., Cohen, R. C., Pusede, S. E., Browne, E. C., Goldstein, A. H., Gentner, D. R., Keutsch, F. N., Thornton, J. A., Harrold, S., Lopez-Hilfiker, F. D., and Wennberg, P. O.: Ozone production chemistry in the presence of urban plumes, Faraday Discuss, 189, 169-189, 10.1039/c5fd00204d, 2016.

Cazorla, M., Brune, W. H., Ren, X., and Lefer, B.: Direct measurement of ozone production rates in Houston in 2009 and comparison with two estimation methods, Atmos Chem Phys, 12, 1203-1212, 10.5194/acp-12-1203-2012, 2012.

Feiner, P. A., Brune, W. H., Miller, D. O., Zhang, L., Cohen, R. C., Romer, P. S., Goldstein, A. H., Keutsch, F. N., Skog, K. M., Wennberg, P. O., Nguyen, T. B., Teng, A. P., DeGouw, J., Koss, A., Wild, R. J., Brown, S. S., Guenther, A., Edgerton, E., Baumann, K., and Fry, J. L.: Testing Atmospheric Oxidation in an Alabama Forest, J Atmos Sci, 73, 4699-4710, 10.1175/Jas-D-16-0044.1, 2016.

Fuchs, H., Bohn, B., Hofzumahaus, A., Holland, F., Lu, K. D., Nehr, S., Rohrer, F., and Wahner, A.: Detection of HO_2 by laser-induced fluorescence: calibration and interferences from RO_2 radicals, Atmos Meas Tech, 4, 1209-1225, 10.5194/amt-4-1209-2011, 2011.

Fuchs, H., Holland, F., and Hofzumahaus, A.: Measurement of tropospheric RO_2 and HO_2 radicals by a laser-induced fluorescence instrument, Rev Sci Instrum, 79, 084104, 10.1063/1.2968712, 2008.

George, I. J., Matthews, P. S., Whalley, L. K., Brooks, B., Goddard, A., Baeza-Romero, M. T., and Heard, D. E.: Measurements of uptake coefficients for heterogeneous loss of HO2 onto submicron inorganic salt aerosols, Phys Chem Chem Phys, 15, 12829-12845, 10.1039/c3cp51831k, 2013.

Grieman, F. J., Noell, A. C., Davis-Van Atta, C., Okumura, M., and Sander, S. P.: Determination of Equilibrium Constants for the Reaction between Acetone and HO2 Using Infrared Kinetic Spectroscopy, The Journal of Physical Chemistry A, 115, 10527-10538, 10.1021/jp205347s, 2011.

Griffith, S. M., Hansen, R. F., Dusanter, S., Michoud, V., Gilman, J. B., Kuster, W. C., Veres, P. R., Graus, M., de Gouw, J. A., Roberts, J., Young, C., Washenfelder, R., Brown, S. S., Thalman, R., Waxman, E., Volkamer, R., Tsai, C., Stutz, J., Flynn, J. H., Grossberg, N., Lefer, B., Alvarez, S. L., Rappenglueck, B., Mielke, L. H., Osthoff, H. D., and Stevens, P. S.: Measurements of hydroxyl and hydroperoxy radicals during CalNex-LA: Model comparisons and radical budgets, J Geophys Res-Atmos, 121, 4211-4232, 10.1002/2015jd024358, 2016.

Griffith, S. M., Hansen, R. F., Dusanter, S., Stevens, P. S., Alaghmand, M., Bertman, S. B., Carroll, M. A., Erickson, M., Galloway, M., Grossberg, N., Hottle, J., Hou, J., Jobson, B. T., Kammrath, A., Keutsch, F. N., Lefer, B. L., Mielke, L. H., O'Brien, A., Shepson, P. B., Thurlow, M., Wallace, W., Zhang, N., and Zhou, X. L.: OH and HO2 radical chemistry during PROPHET 2008 and CABINEX 2009-Part 1: Measurements and model comparison, Atmospheric Chemistry and Physics, 13, 5403-5423, 10.5194/acp-13-5403-2013, 2013.

Hard, T. M., Obrien, R. J., Chan, C. Y., and Mehrabzadeh, A. A.: Tropospheric Free-Radical Determination by Fage, Environ Sci Technol, 18, 768-777, DOI 10.1021/es00128a009, 1984.

Hens, K., Novelli, A., Martinez, M., Auld, J., Axinte, R., Bohn, B., Fischer, H., Keronen, P., Kubistin, D., Nolscher, A. C., Oswald, R., Paasonen, P., Petaja, T., Regelin, E., Sander, R., Sinha, V., Sipila, M., Taraborrelli, D., Ernest, C. T., Williams, J., Lelieveld, J., and Harder, H.: Observation and modelling of HO_x radicals in a boreal forest, Atmospheric Chemistry and Physics, 14, 8723-8747, 10.5194/acp-14-8723-2014, 2014.

Hermans, I., Müller, J.-F., Nguyen, T. L., Jacobs, P. A., and Peeters, J.: Kinetics of α-Hydroxy-alkylperoxyl Radicals in Oxidation Processes. HO2•-Initiated Oxidation of Ketones/Aldehydes near the Tropopause, The Journal of Physical Chemistry A, 109, 4303-4311, 10.1021/jp044080v, 2005.

Hofzumahaus, A., Rohrer, F., Lu, K., Bohn, B., Brauers, T., Chang, C. C., Fuchs, H., Holland, F., Kita, K., Kondo, Y., Li, X., Lou, S., Shao, M., Zeng, L., Wahner, A., and Zhang, Y.: Amplified trace gas removal in the troposphere, Science, 324, 1702-1704, 10.1126/science.1164566, 2009.

Jeanneret, F., Kirchner, F., Clappier, A., van den Bergh, H., and Calpini, B.: Total VOC reactivity in the planetary boundary layer 1. Estimation by a pump and probe OH experiment, J Geophys Res-Atmos, 106, 3083-3093, Doi 10.1029/2000jd900602, 2001.

Jenkin, M. E., Saunders, S. M., Wagner, V., and Pilling, M. J.: Protocol for the development of the Master Chemical Mechanism, MCM v3 (Part B): tropospheric degradation of aromatic volatile organic compounds, Atmos Chem Phys, 3, 181-193, DOI 10.5194/acp-3-181-2003, 2003.

https://doi.org/10.5194/acp-2022-213
Preprint. Discussion started: 4 April 2022


Atmospheric Chemistry and Physics Discussions

Jenkin, M. E., Young, J. C., and Rickard, A. R.: The MCM v3.3.1 degradation scheme for isoprene, Atmos Chem Phys, 15, 11433-11459, 10.5194/acp-15-11433-2015, 2015.

Kleinman, L. I., Daum, P. H., Lee, J. H., Lee, Y. N., Nunnermacker, L. J., Springston, S. R., Newman, L., WeinsteinLloyd, J., and Sillman, S.: Dependence of ozone production on NO and hydrocarbons in the troposphere, Geophys Res Lett, 24, 2299-2302, Doi 10.1029/97gl02279, 1997.

Kleinman, L. I., Daum, P. H., Lee, Y. N., Nunnermacker, L. J., Springston, S. R., Weinstein-Lloyd, J., and Rudolph, J.: Sensitivity of ozone production rate to ozone precursors, Geophys Res Lett, 28, 2903-2906, Doi 10.1029/2000gl012597, 2001.

Lakey, P. S., George, I. J., Baeza-Romero, M. T., Whalley, L. K., and Heard, D. E.: Organics Substantially Reduce HO_2 Uptake onto Aerosols Containing Transition Metal ions, J Phys Chem A, 120, 1421-1430, 10.1021/acs.jpca.5b06316, 2016.

Lakey, P. S., George, I. J., Whalley, L. K., Baeza-Romero, M. T., and Heard, D. E.: Measurements of the HO_2 uptake coefficients onto single component organic aerosols, Environ Sci Technol, 49, 4878-4885, 10.1021/acs.est.5b00948, 2015.

Lakey, P. S. J.: Heteregeneous uptake of HO_2 radicals onto atmospheric aerosols, PhD thesis, School of Chemistry, University of Leeds, 2014.

Lee, J. D., Young, J. C., Read, K. A., Hamilton, J. F., Hopkins, J. R., Lewis, A. C., Bandy, B. J., Davey, J., Edwards, P., Ingham, T., Self, D. E., Smith, S. C., Pilling, M. J., and Heard, D. E.: Measurement and calculation of OH reactivity at a United Kingdom coastal site, J Atmos Chem, 64, 53-76, 10.1007/s10874-010-9171-0, 2009.

Lu, K. D., Hofzumahaus, A., Holland, F., Bohn, B., Brauers, T., Fuchs, H., Hu, M., Häseler, R., Kita, K., Kondo, Y., Li, X., Lou, S. R., Oebel, A., Shao, M., Zeng, L. M., Wahner, A., Zhu, T., Zhang, Y. H., and Rohrer, F.: Missing OH source in a suburban environment near Beijing: observed and modelled OH and HO₂ concentrations in summer 2006, Atmos Chem Phys, 13, 1057-1080, 10.5194/acp-13-1057-2013, 2013.

Lu, K. D., Rohrer, F., Holland, F., Fuchs, H., Bohn, B., Brauers, T., Chang, C. C., Haseler, R., Hu, M., Kita, K., Kondo, Y., Li, X., Lou, S. R., Nehr, S., Shao, M., Zeng, L. M., Wahner, A., Zhang, Y. H., and Hofzumahaus, A.: Observation and modelling of OH and HO_2 concentrations in the Pearl River Delta 2006: a missing OH source in a VOC rich atmosphere, Atmos Chem Phys, 12, 1541-1569, 10.5194/acp-12-1541-2012, 2012.

Mallik, C., Tomsche, L., Bourtsoukidis, E., Crowley, J. N., Derstroff, B., Fischer, H., Hafermann, S., Huser, I., Javed, U., Kessel, S., Lelieveld, J., Martinez, M., Meusel, H., Novelli, A., Phillips, G. J., Pozzer, A., Reiffs, A., Sander, R., Taraborrelli, D., Sauvage, C., Schuladen, J., Su, H., Williams, J., and Harder, H.: Oxidation processes in the eastern Mediterranean atmosphere: evidence from the modelling of HOx measurements over Cyprus, Atmospheric Chemistry and Physics, 18, 10825-10847, 10.5194/acp-18-10825-2018, 2018.

Mao, J., Ren, X., Zhang, L., Van Duin, D. M., Cohen, R. C., Park, J. H., Goldstein, A. H., Paulot, F., Beaver, M. R., Crounse, J. D., Wennberg, P. O., DiGangi, J. P., Henry, S. B., Keutsch, F. N., Park, C., Schade, G. W., Wolfe, G. M., Thornton, J. A., and Brune, W. H.: Insights into hydroxyl measurements and atmospheric oxidation in a California forest, Atmos Chem Phys, 12, 8009-8020, 10.5194/acp-12-8009-2012, 2012.

Mao, J. Q., Ren, X. R., Chen, S. A., Brune, W. H., Chen, Z., Martinez, M., Harder, H., Lefer, B., Rappengluck, B., Flynn, J., and Leuchner, M.: Atmospheric oxidation capacity in the summer of Houston 2006: Comparison with summer measurements in other metropolitan studies, Atmospheric Environment, 44, 4107-4115, 10.1016/j.atmosenv.2009.01.013, 2010.

Mehra, A., Wang, Y., Krechmer, J. E., Lambe, A., Majluf, F., Morris, M. A., Priestley, M., Bannan, T. J., Bryant, D. J., Pereira, K. L., Hamilton, J. F., Rickard, A. R., Newland, M. J., Stark, H., Croteau, P., Jayne, J. T., Worsnop, D. R., Canagaratna, M. R., Wang, L., and Coe, H.: Evaluation of the Chemical Composition of Gas and Particle Phase Products of Aromatic Oxidation, Atmos. Chem. Phys. Discuss., 2020, 1-24, 10.5194/acp-2020-161, 2020.

Moon, D. R.: Heterogeneous reactions involving HO_2 radicals and atmospheric aerosols, PhD thesis, School of Chemistry, University of Leeds, 2018.

Mozurkewich, M., Mcmurry, P. H., Gupta, A., and Calvert, J. G.: Mass Accommodation Coefficient for Ho2 Radicals on Aqueous Particles, J Geophys Res-Atmos, 92, 4163-4170, DOI 10.1029/JD092iD04p04163, 1987.

Niki, H., Maker, P. D., Savage, C. M., and Breitenbach, L. P.: An FTIR study of the Cl-atom-initiated reaction of glyoxal, International Journal of Chemical Kinetics, 17, 547-558, 10.1002/kin.550170507, 1985.

Novelli, A., Hens, K., Ernest, C. T., Kubistin, D., Regelin, E., Elste, T., Plass-Dulmer, C., Martinez, M., Lelieveld, J., and Harder, H.: Characterisation of an inlet pre-injector laser-induced fluorescence instrument for the measurement of atmospheric hydroxyl radicals, Atmos Meas Tech, 7, 3413-3430, 10.5194/amt-7-3413-2014, 2014.

Orlando, J. J. and Tyndall, G. S.: Laboratory studies of organic peroxy radical chemistry: an overview with emphasis on recent issues of atmospheric significance, Chem Soc Rev, 41, 6294-6317, 10.1039/c2cs35166h, 2012.

Orlando, J. J. and Tyndall, G. S.: The atmospheric oxidation of hydroxyacetone: Chemistry of activated and stabilized CH3C(O)CH(OH)OO• radicals between 252 and 298 K, International Journal of Chemical Kinetics, 52, 236-250, 10.1002/kin.21346, 2020.

Osthoff, H. D., Roberts, J. M., Ravishankara, A. R., Williams, E. J., Lerner, B. M., Sommariva, R., Bates, T. S., Coffman, D., Quinn, P. K., Dibb, J. E., Stark, H., Burkholder, J. B., Talukdar, R. K., Meagher, J., Fehsenfeld, F. C., and Brown, S. S.: High levels of nitryl chloride in the polluted subtropical marine boundary layer, Nat Geosci, 1, 324-328, 10.1038/ngeo177, 2008.

Ravishankara, A. R.: Heterogeneous and multiphase chemistry in the troposphere, Science, 276, 1058-1065, DOI 10.1126/science.276.5315.1058, 1997.

Rohrer, F., Lu, K. D., Hofzumahaus, A., Bohn, B., Brauers, T., Chang, C. C., Fuchs, H., Haseler, R., Holland, F., Hu, M., Kita, K., Kondo, Y., Li, X., Lou, S. R., Oebel, A., Shao, M., Zeng, L. M., Zhu, T., Zhang, Y. H., and Wahner, A.: Maximum efficiency in the hydroxyl-radical-based self-cleansing of the troposphere, Nat Geosci, 7, 559-563, 10.1038/Ngeo2199, 2014.

Sadanaga, Y., Yoshino, A., Watanabe, K., Yoshioka, A., Wakazono, Y., Kanaya, Y., and Kajii, Y.: Development of a measurement system of OH reactivity in the atmosphere by using a laser-induced pump and probe technique, Review of Scientific Instruments, 75, 2648-2655, 10.1063/1.1775311, 2004.

Slater, E. J., Whalley, L. K., Woodward-Massey, R., Ye, C., Lee, J. D., Squires, F., Hopkins, J. R., Dunmore, R. E., Shaw, M., Hamilton, J. F., Lewis, A. C., Crilley, L. R., Kramer, L., Bloss, W., Vu, T., Sun, Y., Xu, W., Yue, S., Ren, L., Acton, W. J. F., Hewitt, C. N., Wang, X., Fu, P., and Heard, D. E.: Elevated levels of OH observed in haze events during wintertime in central Beijing, Atmos. Chem. Phys. Discuss., 2020, 1-43, 10.5194/acp-2020-362, 2020.

Sommariva, R., Hollis, L. D. J., Sherwen, T., Baker, A. R., Ball, S. M., Bandy, B. J., Bell, T. G., Chowdhury, M. N., Cordell, R. L., Evans, M. J., Lee, J. D., Reed, C., Reeves, C. E., Roberts, J. M., Yang, M., and Monks, P. S.: Seasonal and geographical variability of nitryl chloride and its precursors in Northern Europe, 19, e844, https://doi.org/10.1002/asl.844, 2018.

Stone, D., Whalley, L. K., and Heard, D. E.: Tropospheric OH and HO_2 radicals: field measurements and model comparisons, Chem Soc Rev, 41, 6348-6404, 10.1039/c2cs35140d, 2012.

Stone, D., Whalley, L. K., Ingham, T., Edwards, P. M., Cryer, D. R., Brumby, C. A., Seakins, P. W., and Heard, D. E.: Measurement of OH reactivity by laser flash photolysis coupled with laser-induced fluorescence spectroscopy, Atmos Meas Tech, 9, 2827-2844, 10.5194/amt-9-2827-2016, 2016.

Tan, Z., Lu, K., Hofzumahaus, A., Fuchs, H., Bohn, B., Holland, F., Liu, Y., Rohrer, F., Shao, M., Sun, K., Wu, Y., Zeng, L., Zhang, Y., Zou, Q., Kiendler-Scharr, A., Wahner, A., and Zhang, Y.: Experimental budgets of OH, HO2, and RO2 radicals and implications for ozone formation in the Pearl River Delta in China 2014, Atmos. Chem. Phys., 19, 7129-7150, 10.5194/acp-19-7129-2019, 2019.

Tan, Z. F., Fuchs, H., Lu, K. D., Hofzumahaus, A., Bohn, B., Broch, S., Dong, H. B., Gomm, S., Haseler, R., He, L. Y., Holland, F., Li, X., Liu, Y., Lu, S. H., Rohrer, F., Shao, M., Wang, B. L., Wang, M., Wu, Y. S., Zeng, L. M., Zhang, Y. S., Wahner, A., and Zhang, Y. H.: Radical chemistry at a rural site (Wangdu) in the North China Plain: observation and model calculations of OH, HO_2 and RO_2 radicals, Atmos Chem Phys, 17, 663-690, 10.5194/acp-17-663-2017, 2017.

Tan, Z. F., Rohrer, F., Lu, K. D., Ma, X. F., Bohn, B., Broch, S., Dong, H. B., Fuchs, H., Gkatzelis, G. I., Hofzumahaus, A., Holland, F., Li, X., Liu, Y., Liu, Y. H., Novelli, A., Shao, M., Wang, H. C., Wu, Y. S., Zeng, L. M., Hu, M., Kiendler-Scharr, A., Wahner, A., and Zhang, Y. H.: Wintertime photochemistry in Beijing: observations of RO_x radical concentrations in the North China Plain during the BEST-ONE campaign, Atmos Chem Phys, 18, 12391-12411, 10.5194/acp-18-12391-2018, 2018.

Tomas, A., Villenave, E., and Lesclaux, R.: Reactions of the HO2 Radical with CH3CHO and CH3C(O)O2 in the Gas Phase, The Journal of Physical Chemistry A, 105, 3505-3514, 10.1021/jp003762p, 2001.

Veyret, B., Lesclaux, R., Rayez, M. T., Rayez, J. C., Cox, R. A., and Moortgat, G. K.: Kinetics and mechanism of the photo-oxidation of formaldehyde. 1. Flash photolysis study, The Journal of Physical Chemistry, 93, 2368-2374, 10.1021/j100343a033, 1989.

Whalley, L. K., Blitz, M. A., Desservettaz, M., Seakins, P. W., and Heard, D. E.: Reporting the sensitivity of laser-induced fluorescence instruments used for HO_2 detection to an interference from RO_2 radicals and introducing a novel approach that enables HO_2 and certain RO_2 types to be selectively measured, Atmos Meas Tech, 6, 3425-3440, 10.5194/amt-6-3425-2013, 2013.

https://doi.org/10.5194/acp-2022-213
Preprint. Discussion started: 4 April 2022

Whalley, L. K., Edwards, P. M., Furneaux, K. L., Goddard, A., Ingham, T., Evans, M. J., Stone, D., Hopkins, J. R., Jones, C. E., Karunaharan, A., Lee, J. D., Lewis, A. C., Monks, P. S., Moller, S. J., and Heard, D. E.: Quantifying the magnitude of a missing hydroxyl radical source in a tropical rainforest, Atmos Chem Phys, 11, 7223-7233, 10.5194/acp-11-7223-2011, 2011.

Whalley, L. K., Slater, E. J., Woodward-Massey, R., Ye, C., Lee, J. D., Squires, F., Hopkins, J. R., Dunmore, R. E., Shaw, M., Hamilton, J. F., Lewis, A. C., Mehra, A., Worrall, S. D., Bacak, A., Bannan, T. J., Coe, H., Ouyang, B., Jones, R. L., Crilley, L. R., Kramer, L. J., Bloss, W. J., Vu, T., Kotthaus, S., Grimmond, S., Sun, Y., Xu, W., Yue, S., Ren, L., Acton, W. J. F., Hewitt, C. N., Wang, X., Fu, P., and Heard, D. E.: Evaluating the sensitivity of radical chemistry and ozone formation to ambient VOCs and NOx in Beijing, Atmos. Chem. Phys. Discuss., 2020, 1-41, 10.5194/acp-2020-785, 2020.

Whalley, L. K., Stone, D., Dunmore, R., Hamilton, J., Hopkins, J. R., Lee, J. D., Lewis, A. C., Williams, P., Kleffmann, J., Laufs, S., Woodward-Massey, R., and Heard, D. E.: Understanding in situ ozone production in the summertime through radical observations and modelling studies during the Clean air for London project (ClearfLo), Atmos Chem Phys, 18, 2547-2571, 10.5194/acp-18-2547-2018, 2018.

Woodward-Massey, R., Slater, E. J., Alen, J., Ingham, T., Cryer, D. R., Stimpson, L. M., Ye, C., Seakins, P. W., Whalley, L. K., and Heard, D. E.: Implementation of a chemical background method for atmospheric OH measurements by laser-induced fluorescence: characterisation and observations from the UK and China, Atmos. Meas. Tech., 13, 3119-3146, 10.5194/amt-13-3119-2020, 2020.

Woodward-Massey, R., Sommariva, R., Whalley, L. K., Cryer, D. R., Ingham, T., Bloss, W. J., Cox, S., Lee, J. D., Reed, C., Crilley, L. R., Kramer, L. J., Bandy, B. J., Forster, G. L., Reeves, C. E., Monks, P. S., and Heard, D. E.: Radical chemistry at a UK coastal receptor site – Part 1: observations of OH, HO2, RO2, and OH reactivity and comparison to MCM model predictions, Submitted, 2022.

Worton, D. R., Reeves, C. E., Penkett, S. A., Sturges, W. T., Slemr, J., Oram, D. E., Bandy, B. J., Bloss, W. J., Carslaw, N., Davey, J., Emmerson, K. M., Gravestock, T. J., Hamilton, J. F., Heard, D. E., Hopkins, J. R., Hulse, A., Ingram, T., Jacob, M. J., Lee, J. D., Leigh, R. J., Lewis, A. C., Monks, P. S., and Smith, S. C.: Alkyl nitrate photochemistry during the tropospheric organic chemistry experiment, Atmospheric Environment, 44, 773-785, https://doi.org/10.1016/j.atmosenv.2009.11.038, 2010.

Zhao, Y., Thornton, J. A., and Pye, H. O. T.: Quantitative constraints on autoxidation and dimer formation from direct probing of monoterpene-derived peroxy radical chemistry, Proc Natl Acad Sci U S A, 115, 12142-12147, 10.1073/pnas.1812147115, 2018.

https://doi.org/10.5194/acp-2022-213
Preprint. Discussion started: 4 April 2022

Atmospheric Chemistry and Physics Discussions

Tables

Table 1. Median daytime (defined as $J(O^1D) > 5 \times 10^{-7}$ s^{-1}, approximately 06:00–18:00 UTC) RO_x source and sink contributions, split according to wind direction (NW–SE = <165° and >285°; SW = 180°–270°).

RO_x source	NW–SE (%)	SW (%)	*RO_x sink*	NW–SE (%)	SW (%)
Ozonolysis	3.1	2.8	$RO_2 + NO \rightarrow RONO_2$	28.1	38.2
$J_{carbonyls}$	22.9	24.5	$HO_2 + HO_2$	1.8	0.9
J_{HONO}	36.5	44.0	$RO_2 + HO_2$	32.6	14.2
$O^1D + H_2O$	37.5	28.7	$RO_2 + RO_2$	1.5	1.1
			$OH + NO_2$	32.6	39.4
			OH + NO	3.4	6.2

Table 2. Median daytime OH source and sink contributions, split according to wind direction. OH reactivity contributions are derived from calculated OH reactivity, not measured. OH sink groupings are based on MCM classifications.

OH source	NW–SE (%)	SW (%)	*OH sink*	NW–SE (%)[a]	SW (%)[b]
Ozonolysis	0.8	0.5	Aromatics[c]	0.4	0.3
$O^1D + H_2O$	23.2	11.5	HONO[c]	0.7	0.7
J_{HONO}	22.6	17.7	Methanol[c]	1.7	3.1
$HO_2 + O_3$	2.4	0.9	Alkanes[c]	2.5	1.6
$HO_2 + NO$	51.0	69.4	NO	2.7	4.5
			Unclassified[c]	2.7	1.8
			O_3[c]	3.0	2.3
			Dialkenes (isoprene + 1,3-butadiene)	4.2	5.5
			Alkenes + alkynes	7.9	6.4
			Carbonyls	13.0	20.9
			NO_2	19.5	26.2
			CO	41.6	26.7

[a]Median missing reactivity = 2.2 s^{-1} (48% of measured).

[b]Median missing reactivity = 2.4 s^{-1} (49% of measured).

[c]Lumped together as “others” in Figure 8.

https://doi.org/10.5194/acp-2022-213
Preprint. Discussion started: 4 April 2022

Atmospheric Chemistry and Physics Discussions

Figures

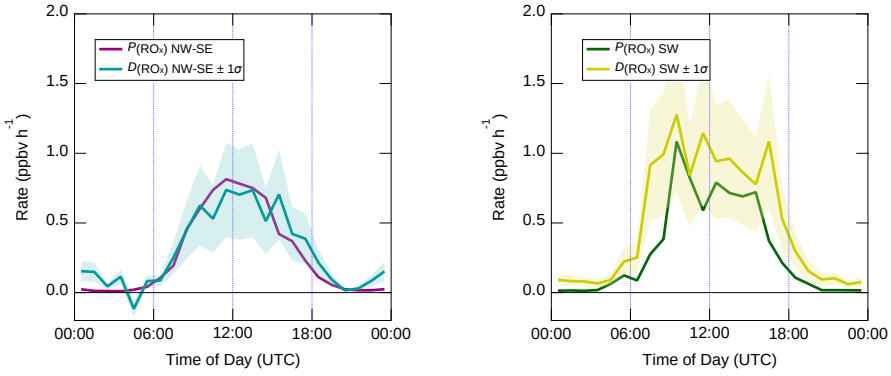

Figure 1. Median diel profiles of RO_x production and destruction, split according to wind direction (NW–SE = <165° and >285°; SW = 180°–270°). Shaded area on $D(RO_x)$ corresponds to the estimated 1σ uncertainty of 35% (derived from calibration accuracy and reproducibility), not shown for $P(RO_x)$ for clarity.

5

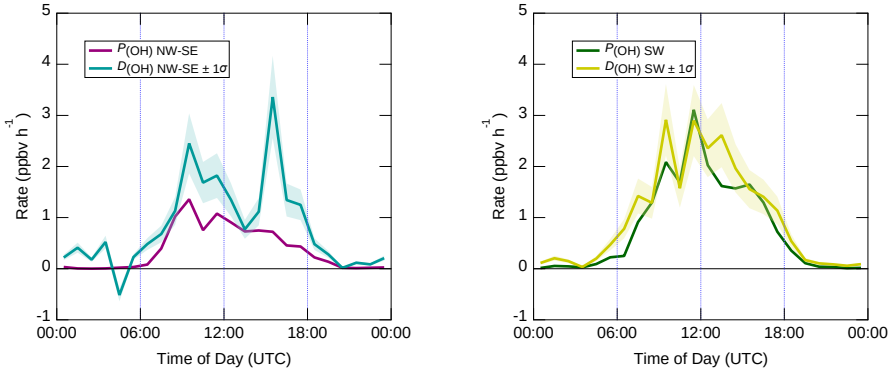

Figure 2. Median diel profiles of OH production and destruction, split according to wind direction. Shaded area on D(OH) corresponds to the estimated 1σ uncertainty of 24%, not shown for P(OH) for clarity.

https://doi.org/10.5194/acp-2022-213
Preprint. Discussion started: 4 April 2022

Atmospheric Chemistry and Physics Discussions

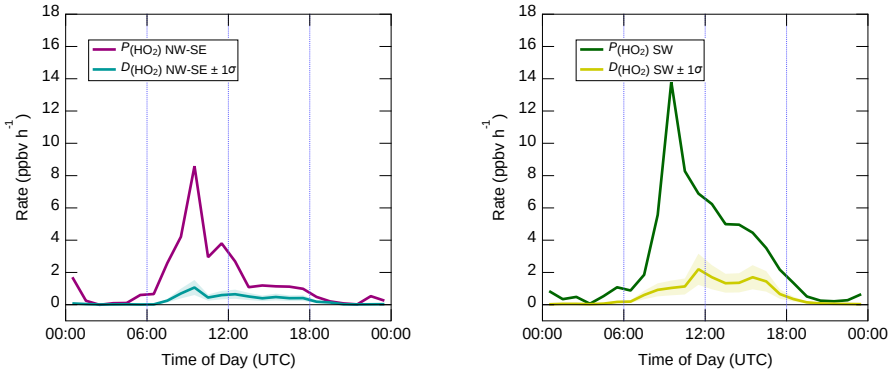

Figure 3. Median diel profiles of HO_2 production and destruction, split according to wind direction. Shaded area on $D(HO_2)$ corresponds to the estimated 1σ uncertainty of 32%, not shown for $P(HO_2)$ for clarity.

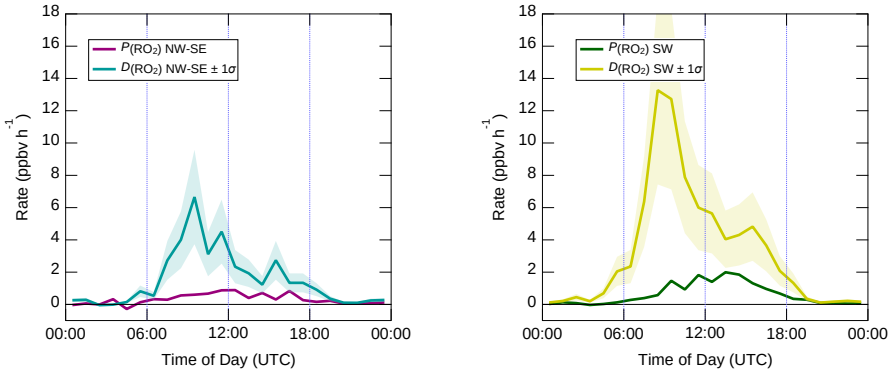

Figure 4. Median diel profiles of RO_2 production and destruction, split according to wind direction. Shaded area on $D(RO_2)$ corresponds to the estimated 1σ uncertainty of 32%, not shown for $P(RO_2)$ for clarity.

https://doi.org/10.5194/acp-2022-213
Preprint. Discussion started: 4 April 2022

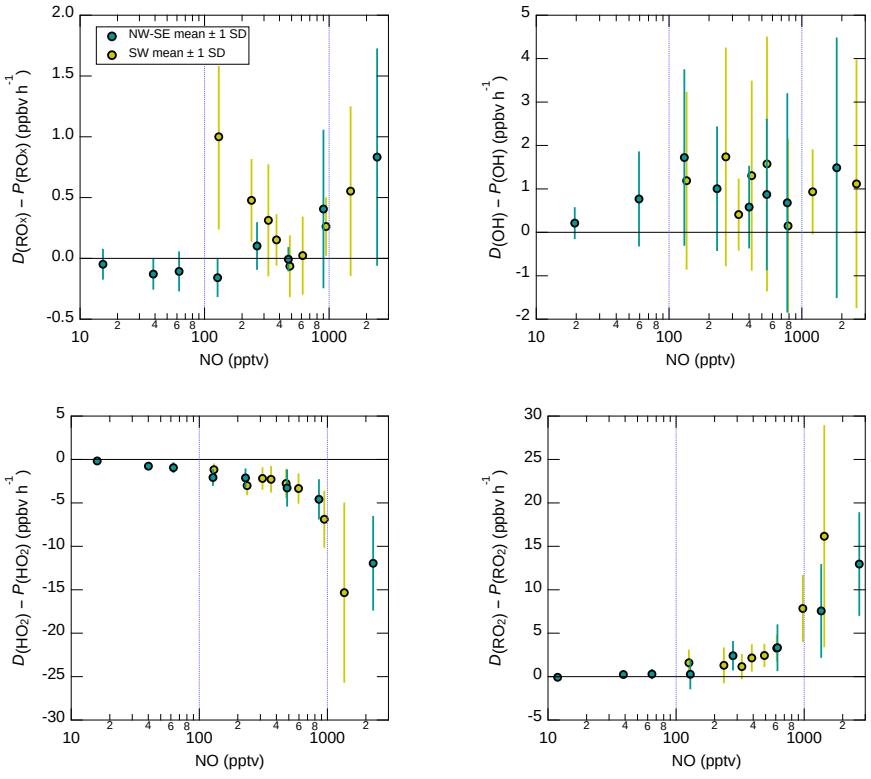

Figure 5. Destruction minus production (i.e., budget imbalance) as a function of NO for RO_x (top left), OH (top right), HO_2 (bottom left), and RO_2 (bottom right) in NW–SE and SW air. Daytime points only, with daytime defined as $J(O^1D) > 5 \times 10^{-7}$ s^{-1}. Data were separated into 8 bins with an approximately equal number of points. Data points are shown as means ± one standard deviation (SD). Note *x*-log scale.

https://doi.org/10.5194/acp-2022-213
Preprint. Discussion started: 4 April 2022

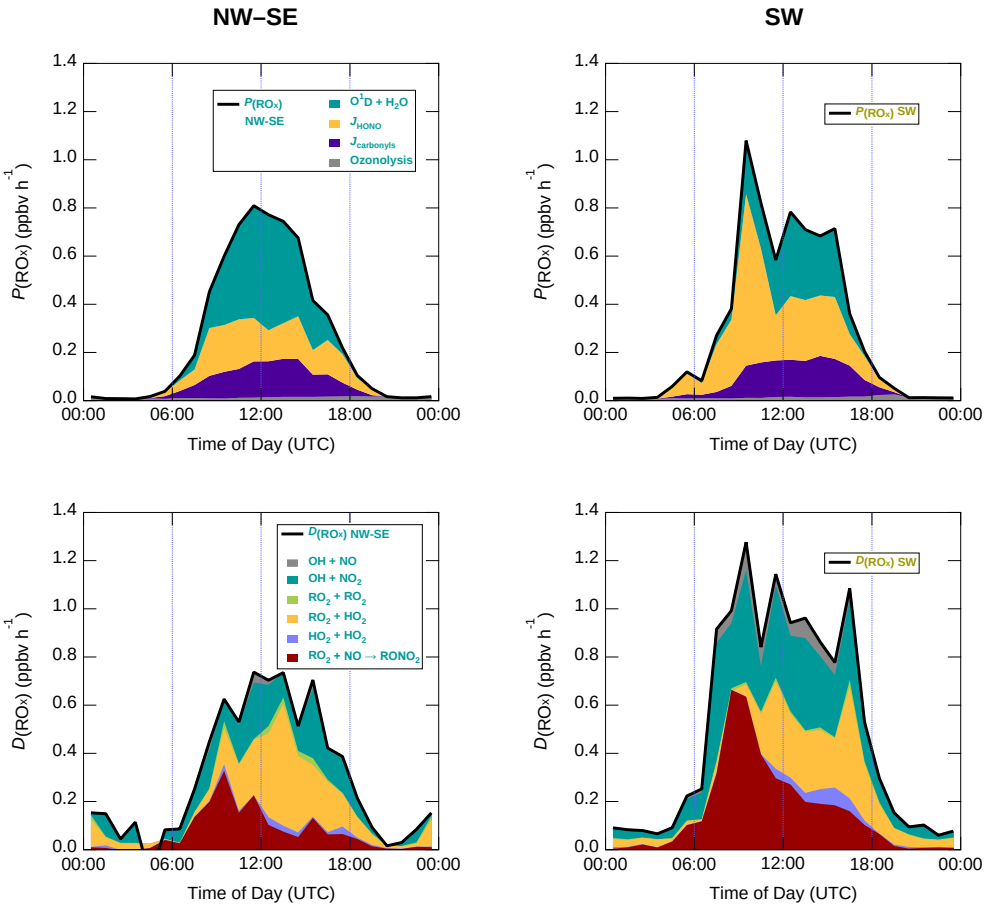

Figure 6. Median diel profiles of known RO_x sources (top) and sinks (bottom), split according to wind direction. Average daytime contributions are given in Table 1. For interpretation of colours, please see the figure legend.

https://doi.org/10.5194/acp-2022-213
Preprint. Discussion started: 4 April 2022

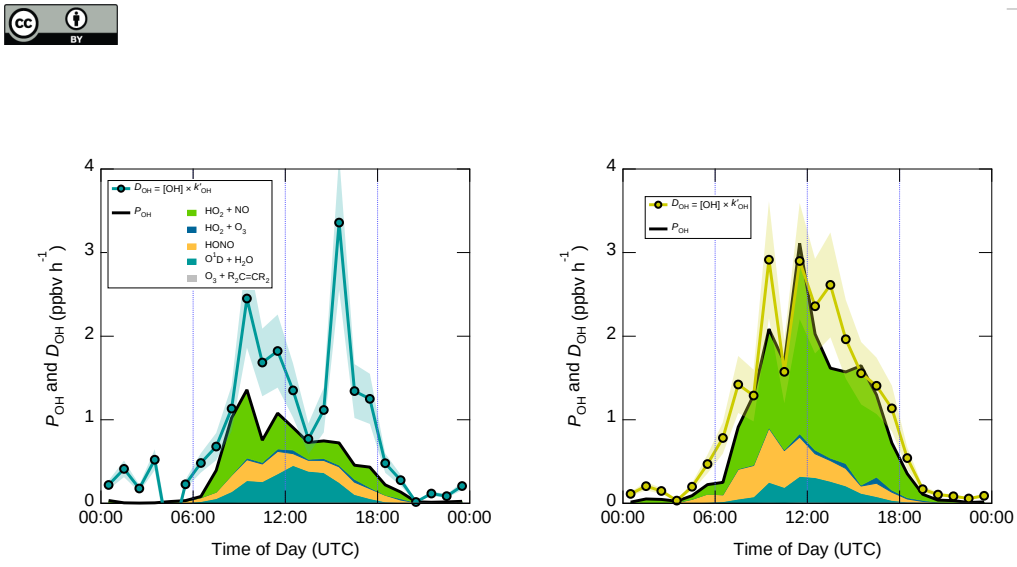

Figure 7. Median diel profiles of known OH sources and comparison to measured OH destruction, split according to wind direction (left: NW–SE, right: SW). Average daytime contributions are given in Table 2. For interpretation of colours, please see the figure legend.

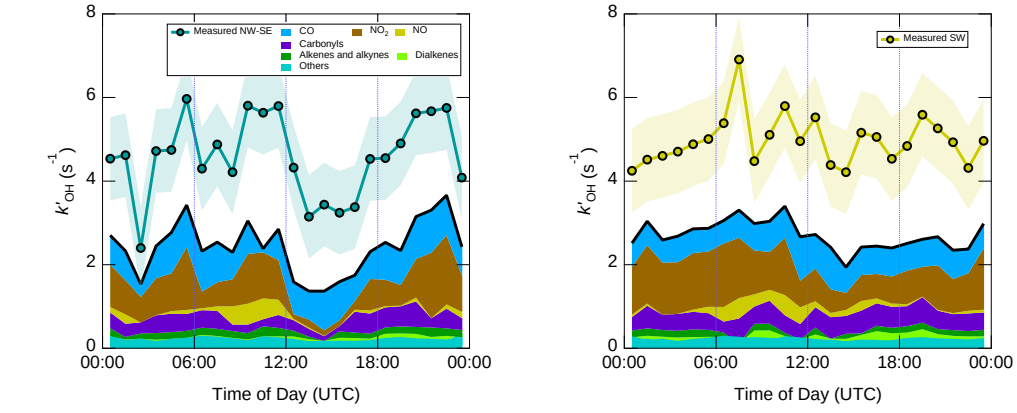

Figure 8. Median diel profiles of the OH reactivity calculated from measured reactants and comparison to measured OH reactivity, split according to wind direction. Average daytime contributions are given in Table 2. For interpretation of colours, please see the figure legend. Reactants in the "others" class are listed in Table 2. The shaded area on measured k'_{OH} corresponds to the 1σ precision of ~1 s^{-1}. Model intermediates are not included here but their contributions may be found in our companion paper (Woodward-Massey et al., 2022).

https://doi.org/10.5194/acp-2022-213
Preprint. Discussion started: 4 April 2022

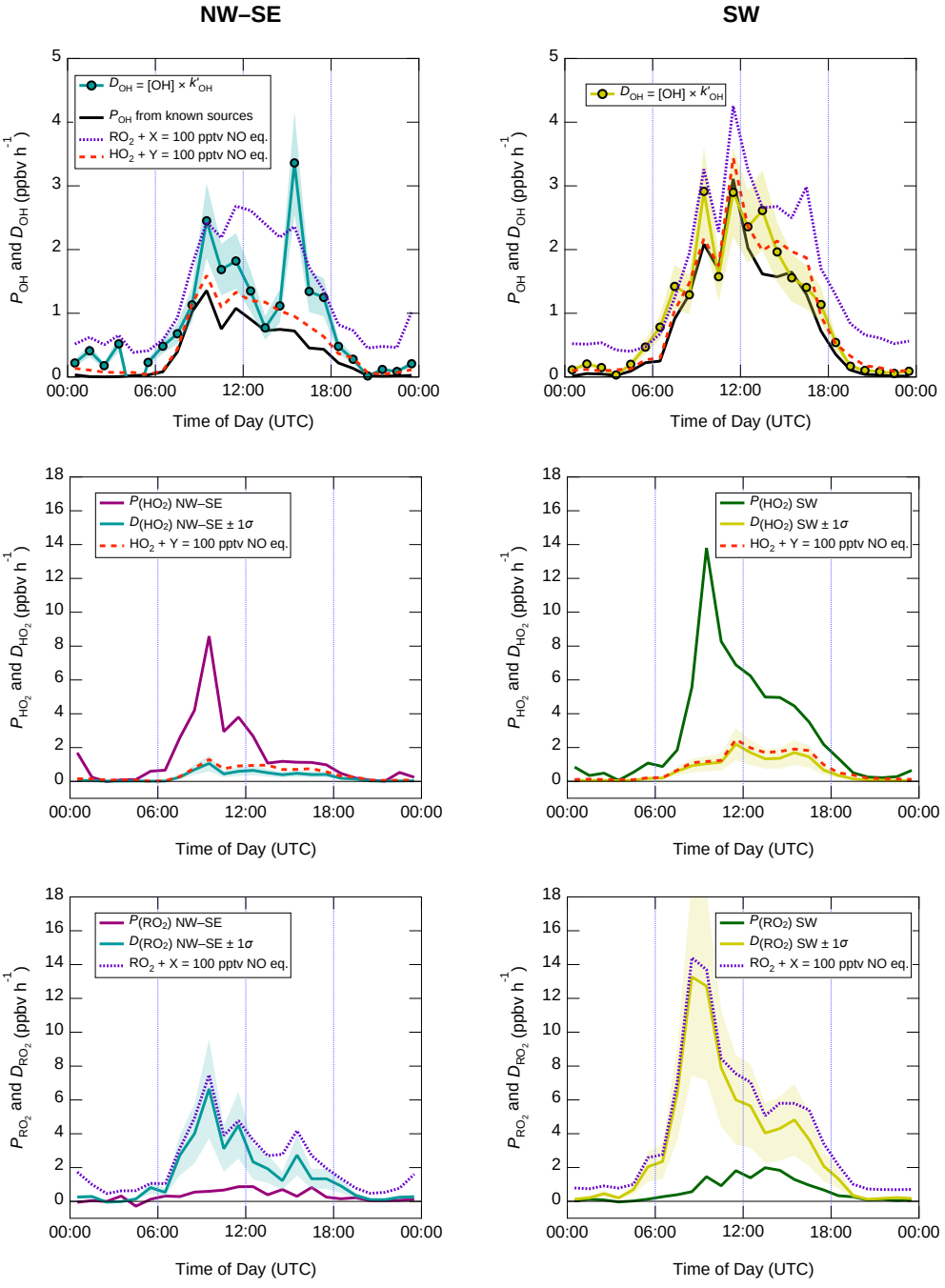

Figure 9. OH, HO_2, and RO_2 budgets with inclusion of additional radical recycling from species "X" and "Y", where RO_2 + X → OH and HO_2 + Y → OH. In each case, X and Y were set to a constant 100 pptv and assumed to react with the same rate constants as RO_2 + NO and HO_2 + NO, respectively ("eq." = equivalent).

https://doi.org/10.5194/acp-2022-213
Preprint. Discussion started: 4 April 2022

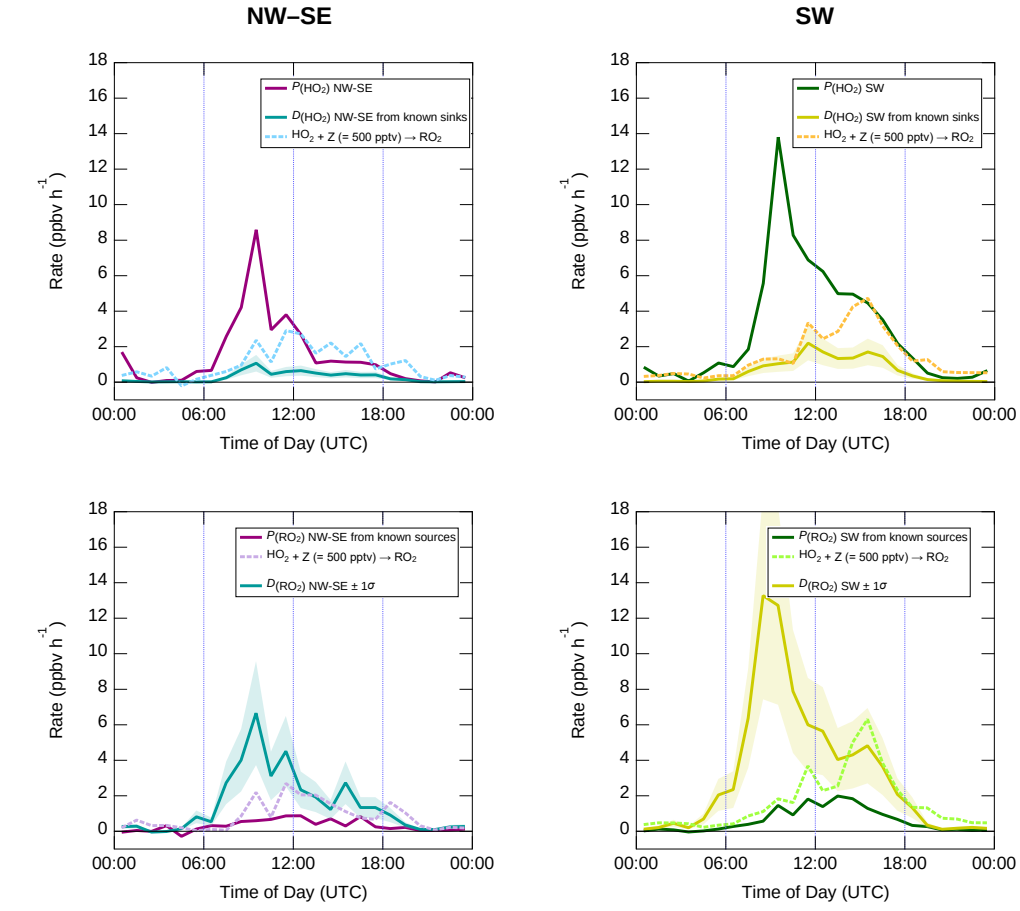

Figure 10. HO_2 (top) and RO_2 (bottom) budgets with inclusion of additional radical propagation from species "Z", where $HO_2 + Z \rightarrow RO_2$. Z was set to a constant 500 pptv and assumed to react with the same rate constant as $HO_2 + NO$.

https://doi.org/10.5194/acp-2022-213
Preprint. Discussion started: 4 April 2022

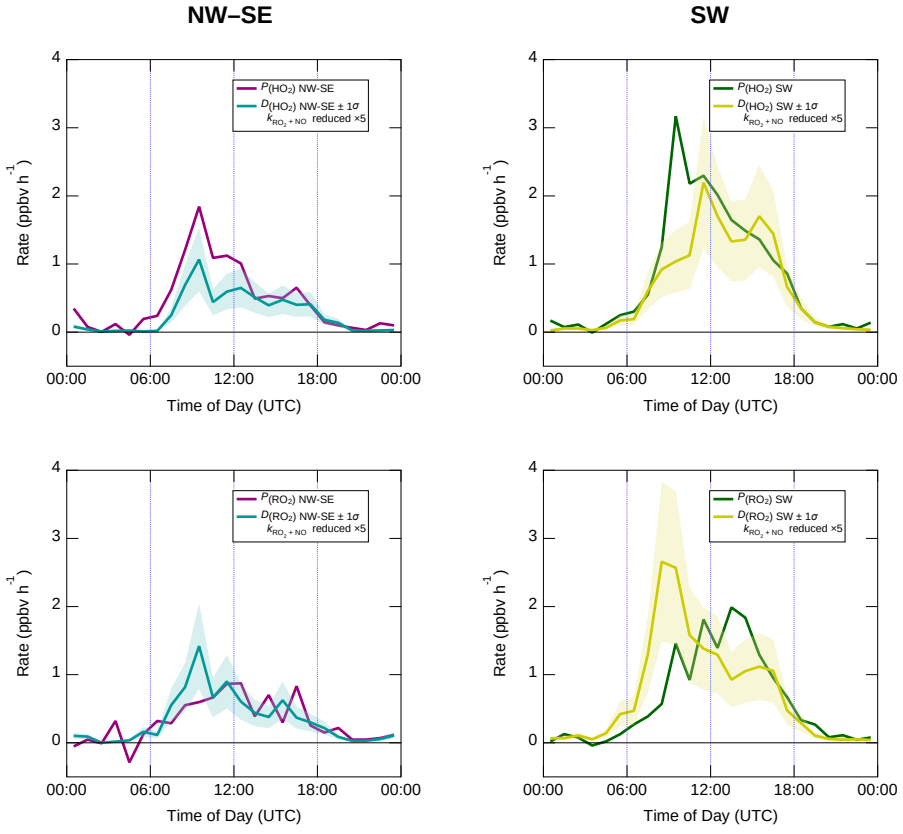

Figure 11. HO_2 (top) and RO_2 (bottom) budgets after artificially reducing the RO_2 + NO rate constant by a factor of 5.

https://doi.org/10.5194/acp-2022-213
Preprint. Discussion started: 4 April 2022

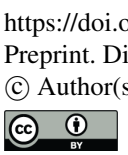

Atmospheric Chemistry and Physics Discussions

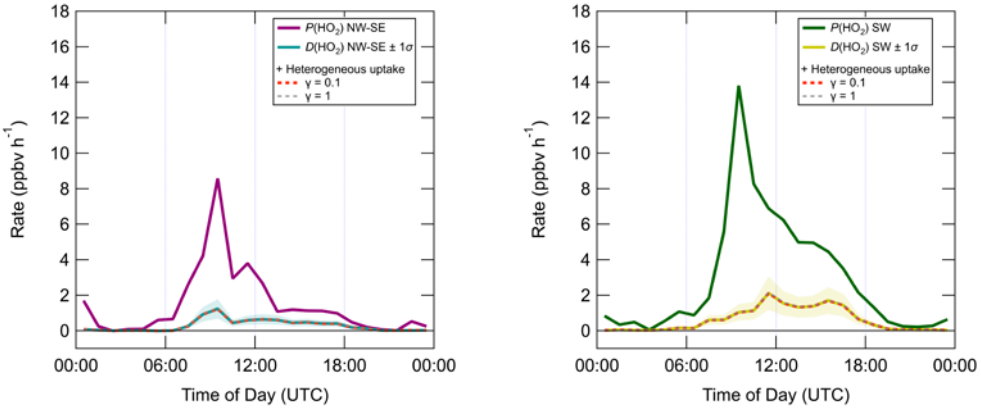

Figure 12. HO_2 budget after inclusion of heterogeneous uptake using different γ_{HO2}.

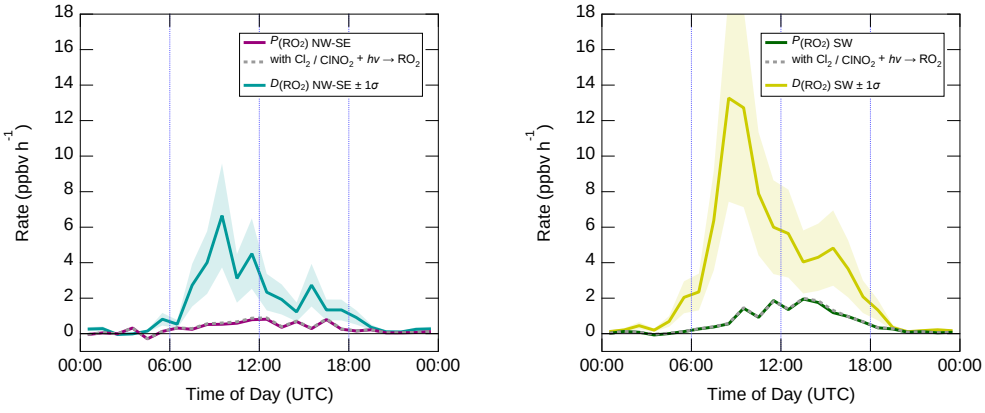

Figure 13. RO_2 budget after inclusion of chlorine chemistry. All photolysed Cl atoms are assumed to react with VOCs to yield RO_2, i.e., $Cl_2/ClNO_2 \rightarrow nCl \rightarrow nRO_2$, where $n = 2$ for Cl_2 and $n = 1$ for $ClNO_2$. This assumption therefore yields an upper limit for the impact of chlorine chemistry.

https://doi.org/10.5194/acp-2022-213
Preprint. Discussion started: 4 April 2022

Atmospheric Chemistry and Physics Discussions

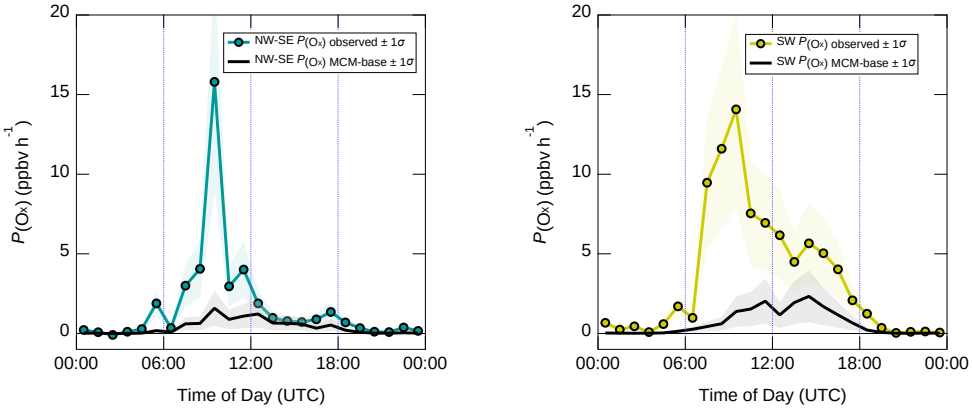

Figure 14. Median diel profiles of $P(O_x)$, defined in equations (E12–E14), as calculated from measured and MCM-base model HO_2 and RO_2, split according to wind direction. Shaded areas correspond to estimated 1σ uncertainties of 40% and 70% for measured and model $P(O_x)$, respectively.

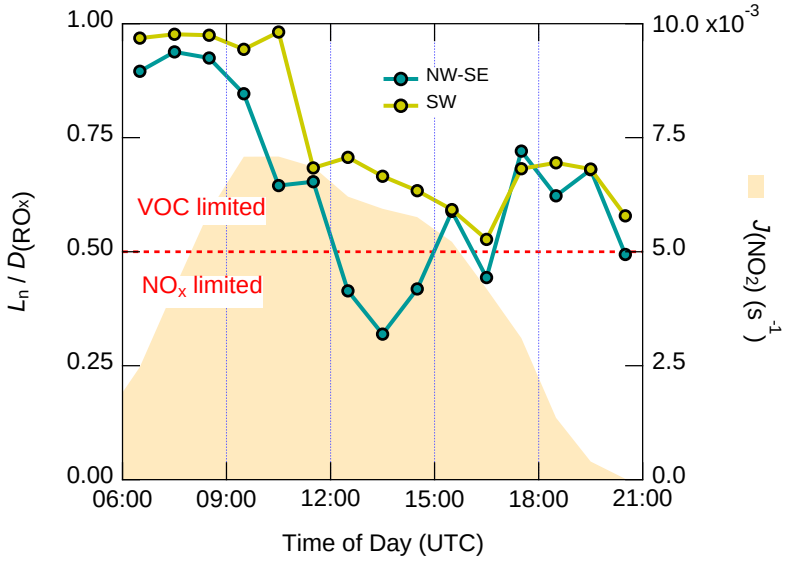

Figure 15. Daytime (06:00–21:00 UTC) ozone production regime based on the ratio L_n / $D(RO_x)$ (left axis). $J(NO_2)$ is shown on the right axis. The dashed line corresponds to the transition between VOC and NO_x limited ozone production (L_n / $D(RO_x)$ = 0.5).

https://doi.org/10.5194/acp-2022-213
Preprint. Discussion started: 4 April 2022

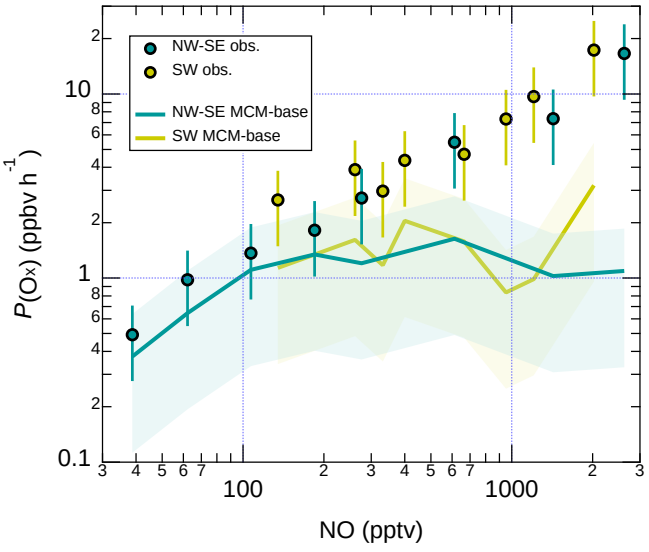

Figure 16. $P(O_x)$ as a function of NO for measured and MCM-base model HO_2 and RO_2. Error bars and shaded areas correspond to estimated 1σ uncertainties of 40% and 70% for measured and model $P(O_x)$, respectively. Note *y*- and *x*-log scales.